Report
P-19-12
December 2019

Development of thermo-hydraulic model for pellet fillings

Peter Eriksson

SVENSK KÄRNBRÄNSLEHANTERING AB

SWEDISH NUCLEAR FUEL
AND WASTE MANAGEMENT CO

Box 3091, SE-169 03 Solna
Phone +46 8 459 84 00
skb.se

SVENSK KÄRNBRÄNSLEHANTERING

ISSN 1651-4416
SKB P-19-12
ID 1869758
December 2019

Development of thermo-hydraulic model for pellet fillings

Peter Eriksson
Svensk Kärnbränslehantering AB

Abstract

A model to describe water transport in bentonite pellet fillings has been developed. The model handles much of the physics that could occur in the pellet fillings such as suction gradient driven water transport, vapour transport through diffusion and convection and flow of water in the void space in between the pellets. One limitation of the model is that it currently cannot predict the formation of pipes and the influence this has on the transport properties.

Sammanfattning

En modell för att beskriva hur vattentransport i fyllningar av bentonitpelletar har utvecklats. Modellen kan hantera mycket av den fysik som kan förekomma i pelletfyllningar som till exempel vattentransport på grund av skillnader i osmotisk potential, ångtransport genom diffusion och genom konvektion samt flöde av vatten i håligheterna mellan pelletarna. En begränsning med modellen är att den i dagsläget inte kan fånga fenomenet med piping och hur det påverkar transportegenskaperna.

Contents

1 Introduction

In the KBS3 system a copper canister is deposited in a deposition hole surrounded by a bentonite buffer. The buffer is made of both compacted bentonite blocks and bentonite pellets with the pellets placed between the bentonite blocks and the rock. There will be water inflow from the rock and a redistribution of water due to the temperature gradient caused by the hot canister. The pellet filling will therefore influence the saturation process especially during the early stages. The deposition tunnels are then backfilled with bentonite blocks and pellets. Bentonite pellets are therefore used in both the backfill and the buffer. The models to describe the pellet fillings mathematically has had limited capabilities and work has therefore been done to try and improve it.

It is desirable to be able to predict how the system behaves under different conditions during the early stages after installation because this will affect how the installation process is being designed and what constrains there will be on the installation. One way of doing this is with modelling. Modelling of the bentonite blocks is relatively well developed and tested but, the pellet slot is more complicated to model. To be able to model the behaviour during the early stage it is essential to be able to model how water and vapour is transported in the pellet-filled slot. To increase the capability to model pellet fillings work was initiated in the EBS Task force where some experiments were done as modelling cases.

2 The use of bentonite pellets in the KBS3 system

Bentonite pellets are used in several places in the KBS3 system. The purpose of the pellet fillings is both to increase the installed density and to handle inflowing water. The inflowing water is handled by spreading the water over a larger area and storing it.

In the backfill, pellets are used on the floor as a foundation for the block stack and to fill the space between the block stack and the rock. Pellets are placed on the floor and smoothen to a flat surface. On this flat surface the blocks are then placed. The pellets placed in the deposition tunnel do not have very large thermal gradients and the most important modelling task is therefore to predict transport of water both due to suction gradients and free water transported in between the pellets. The pellets used in the backfill are extruded pellets because they have been found to work better for this application (Johnsson and Sandén 2013).

For the buffer, roller compacted pellets are currently being used between the buffer blocks and the rock. In this part there is also a thermal gradient which redistributes water due to the increased formation of water vapour. In order to set a limit when the deposition hole is considered wet or dry, it is important to get a better prediction of how water moves in the pellet filling. A dry deposition hole will not require any extra attention during installation, whereas for a wet deposition hole a change in the installation sequence is needed so that the time until the installation of backfill can be reduced.

Because pellets were available which have been used for other tests these pellets were used in these tests as well. The pellets types are: extruded pellets made by Asha material and roller compacted which is made by MX80. The two types of pellets are shown in Figure 2-1. Data for the different pellets are shown in Table 2-1.

Table 2-1. Pellet types and basic data for pellets used in the tests to evaluate pellet model.

Pellet type	Material	Particle density, ρs	Water content	Pellet dry density	Bulk dry
Extruded	Asha	2 920 kg/m^3	15.6 %	1 924 kg/m^3	958 kg/m^3
Roller compacted	MX80	2 780 kg/m^3	15 %	1 841 kg/m^3	953 kg/m^3

Figure 2-1. *Extruded pellets made of Asha material to the left and roller compacted pellets from MX80 to the right.*

3 Conceptual description of moisture transport in pellet fillings

3.1 General concept

In this chapter the conceptual model of the moisture transport of pellet fillings is described. The mathematical model developed (see chapter 5) is then based on this conceptual model.

The pellet filling consist of individual pellets stacked on each other with pores in-between them. In real pellets there are also pores inside the pellet but in this work the pellets are considered to be fully water saturated. This will simplify the analisis because there is only one pore space to consider. The pellet filling therefore has two different spaces which have different transport properties, the pore space and the clay space, see Figure 3-1.

In the clay space water can be transported due to differences in suction. There is also a heat transport by conduction in the clay space.

In the pore space fluids can move. These fluids can be either air or water. In the case when the pores are air-filled water vapour will also be present which can be transported in the pore space by diffusion and convection. This water vapour will evaporate from the clay into the air if the relative humidity in the air is lower than the relative humidity in equilibrium with the water in the clay space and condensate when the opposite is true. When free water is moving in the pore space it can be absorbed by the clay space.

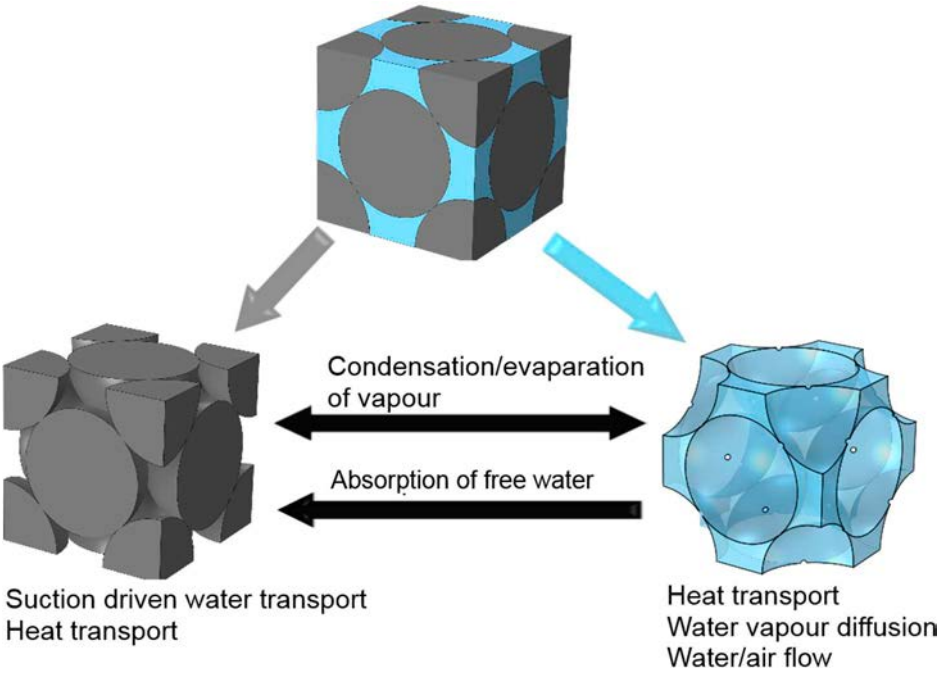

Figure 3-1. *Illustration of the different spaces in the bentonite fillings were transport can take place.*

The individual pellets are in contact with each other in small points. Everything that is transported in the clay space need to pass these small contact points as illustrated in Figure 3-2. It is therefore assumed that these contacts points are the limiting factor for the transport properties in the clay space.

As the pellets absorb moisture from its surrounding it will start to swell and close the pore space between the pellets. The swelling rate is limited by the rate it can absorb the water. Therefore water can flow in this pore space before the pore space closes and the system behaves like a solid piece of bentonite. In this concept it is assumed that there is no mechanical interaction between the individual pellets and the pellet swells uniformly in all direction, illustrated in Figure 3-3. This will likely underestimate the contact area between the pellets at higher saturation.

Heat transfer in the pellet slot can take place by conduction in the pellets, radiation between individual pellets and by conduction in the air-filled pore space between the pellets. If the air in the pellet space is moving due to external forces or thermal gradients there will also be heat transfer caused by convection.

The heat transfer due to radiation, conduction in the air-filled inter-pellet pore space and convection is related to the shape and size of the pores between the pellets. The conduction part in the pellets is determined by the area of the contact point between the pellets.

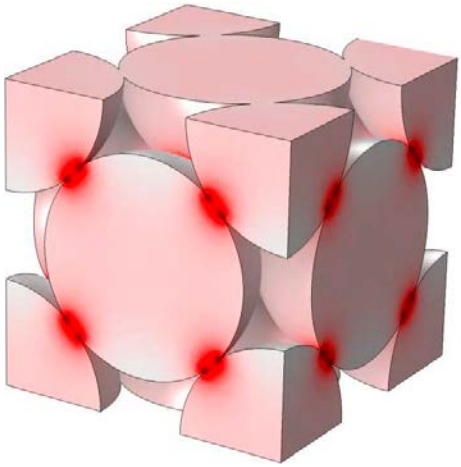

Figure 3-2. *Heat fluxes in a pellet filling (darker red is higher flux) which illustrate that the contact points between the pellets are the limiting factor for transport of e.g. heat.*

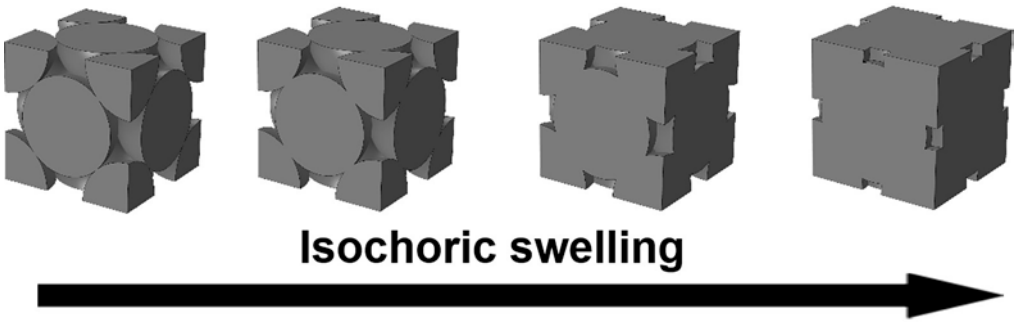

Figure 3-3. *Swelling of the pellet filling when the volume is kept constant.*

4 Modelling of unit cells

4.1 General

In order to examine the properties of the pellet fillings a number of calculations are done on a smaller scale with individual pellets present in the model. In order to get small models this modelling is done on unit cells in which symmetry boundary conditions can be used. Even if the ordered structure of the unit cells does not completely match to geometry of a random packing this modelling should give a good estimation of the properties on a smaller scale. Furthermore, to get the ordered structure the assumption the pellets are spherical need to be done. The shape of the pellets will most likely affect the properties but this is not considered in this modelling.

The unit cells used in the modelling would be diamond cubic (DC), simple cubic (SC) and face centered cubic (FCC). These unit cells are shown in Figure 4-1. The packing density and therefore also the inter-pellet porosity is well known for these unit cells and therefore the corresponding dry density can be calculated with Equation 4-1. These unit cells would correspond to dry densities of 670 kg/m^3 (DC), 1 025 kg/m^3 (SC) and 1 460 kg/m^3 (FCC) respectively if a water content of 15 % and full saturation of the individual pellets is assumed. The simple cubic is therefore the unit cell which most closely resembles the random packing of the pellet fillings which can have a dry density from approximately 850 kg/m^3 to approximately 1 100 kg/m^3 with a typical value around 950 kg/m.

$$\rho_d = \frac{(1-\varphi_a)}{\left(\frac{1}{\rho_s}+\frac{w}{\rho_w}\right)} \qquad \text{Equation 4-1}$$

To represent the swelling of the pellets and the reduced porosity as a consequence of this it is assumed that the pellets swell equally in all directions and that no mechanical interaction between the pellets takes place. The assumed swelling behaviour is illustrated in Figure 3-3.

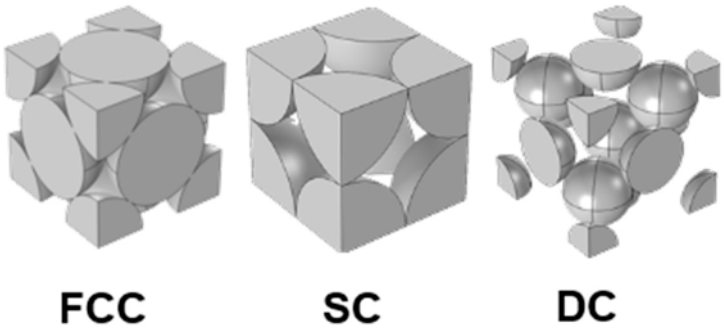

Figure 4-1. *The different unit cells used to model the properties of the pellet filling.*

4.2 Thermal conductivity

The thermal conductivity of the individual pellets is assumed to be equal to the value of saturated bentonite, approximately 1.35 W/m/K and is assumed to be constant and not a function of density which it probably is. However, the density dependence seems to be small when the material is saturated according to measurements (Svensson et al. 2019).

To investigate what the effective thermal conductivity of a pellet filling could be, two types of unit cells are modelled numerically, SC and FCC. A thermal gradient is applied over the unit cell and an effective thermal conductivity can be calculated. The result of the numerical modelling can be seen in Figure 4-2. Since the pellet has zero contact area at the initial inter-pellet porosity the thermal conductivity is also zero at the initial condition. This is not completely true because heat can also be transported through the air by thermal radiation and heat conduction. If thermal radiation between the pellets and thermal conduction in the air between the pellets is added to the model the effective thermal conductivity

of the pellet filling will be approximately 0.2 W/mK for an inter-pellet porosity of 0.48 as seen in Figure 4-3. This thermal conduction is dependent on the geometry of the pellet filling and the size of the pores between the pellets and might changes if the pellet type is changed.

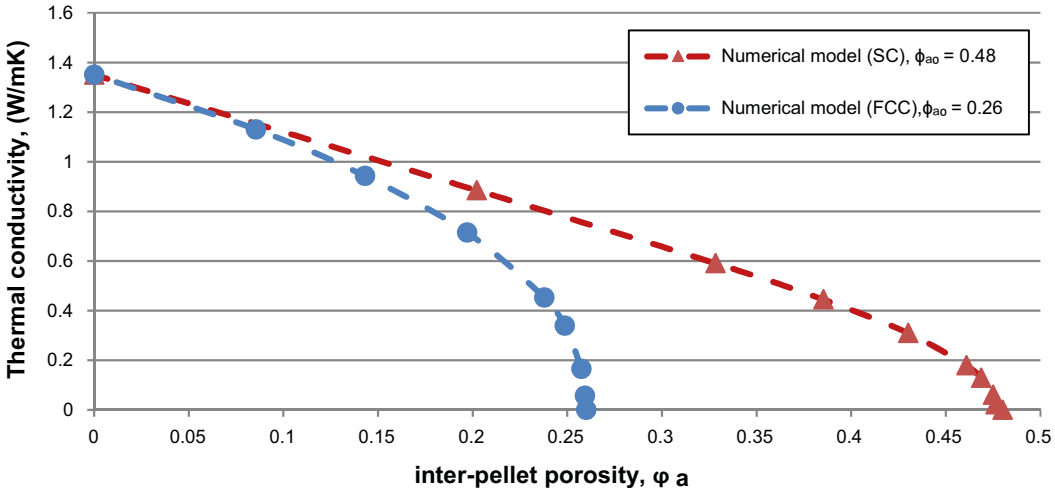

Figure 4-2. *Calculated effective thermal conductivity in two different unit cells, SC and FCC, when only conduction in the pellets is considered.*

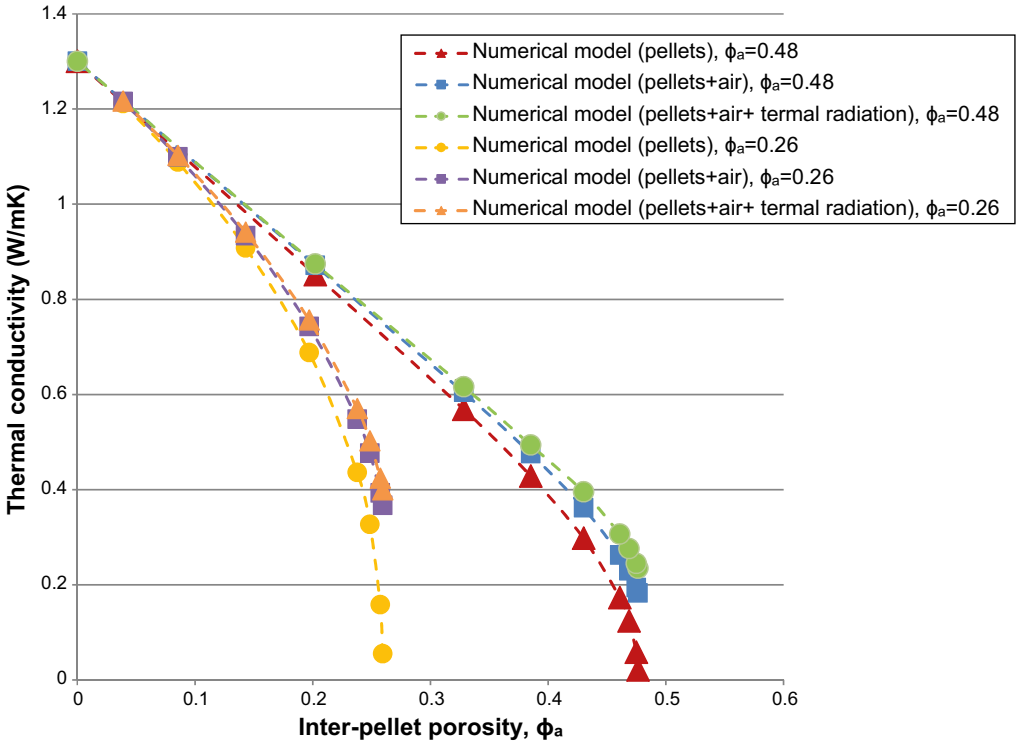

Figure 4-3. *Effective thermal conductivity when all thermal transport physics is considered.*

4.3 Effective vapour diffusion coefficient

Because there are pores in the pellet filling, where the vapour diffusion take place, the diffusion coefficient for water vapour in air cannot be used as it is. Instead an effective diffusion coefficient is used and it is defined as shown in Equation 4-2.

$$D_{eff} = \frac{\varphi_a}{\tau} D_v \qquad \text{Equation 4-2}$$

Where D_{eff} is the effective diffusion coefficient and τ is the tortuosity. To be able to predict the tortuosity the unit cells are modelled with fixed concentration on each side. From this the tortuosity can be calculated and the result is shown in Figure 4-4. The result differs a bit between the different unit cells. In real life the tortuosity would be some kind of average between the different types. It is assumed that the extruded pellets would have the same tortuosity. An empirical expression to predict the tortuosity is proposed, Equation 4-3.

$$\tau = 1 + \frac{0.27}{\varphi_a} \qquad \text{Equation 4-3}$$

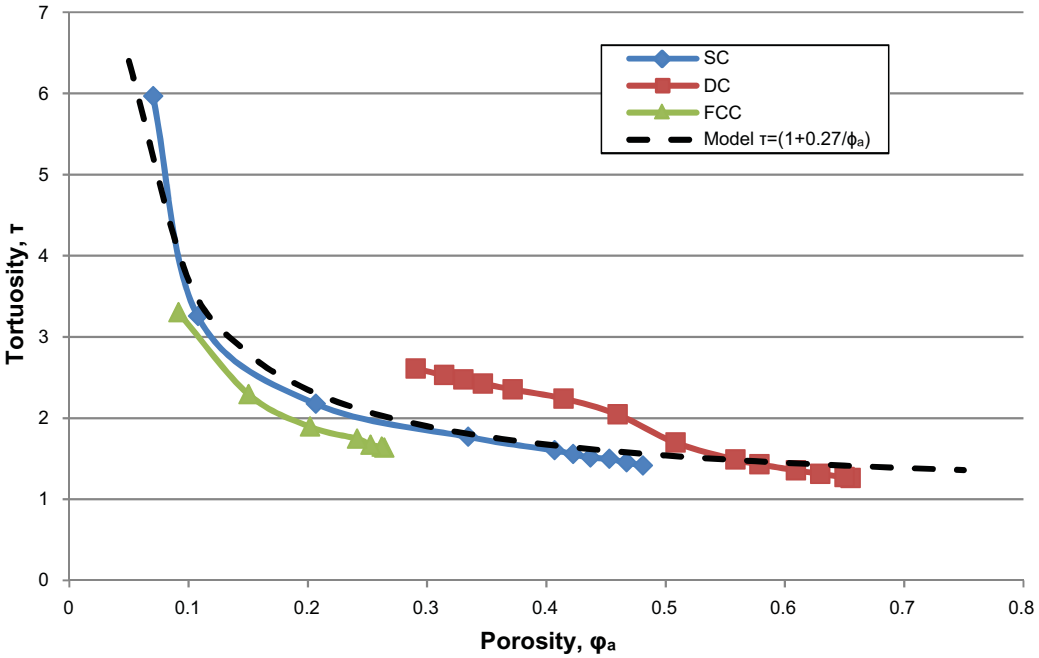

Figure 4-4. *The tortuosity calculated from the different unit cells.*

4.4 Gas flow in between the pellets

Since the models allow flow in the pore space a flow resistance need to be calculated. The flow in the pore space of the SC unit cell has been modelled because this unit cell is expected to be the ones that are closest to the pellet fillings modelled in this report. The modelling shows that the flow resistance is dependent not only on porosity but also on the size of the individual pores. The calculated flow resistance is shown in Figure 4-5 for different sizes of the pores between the pellets

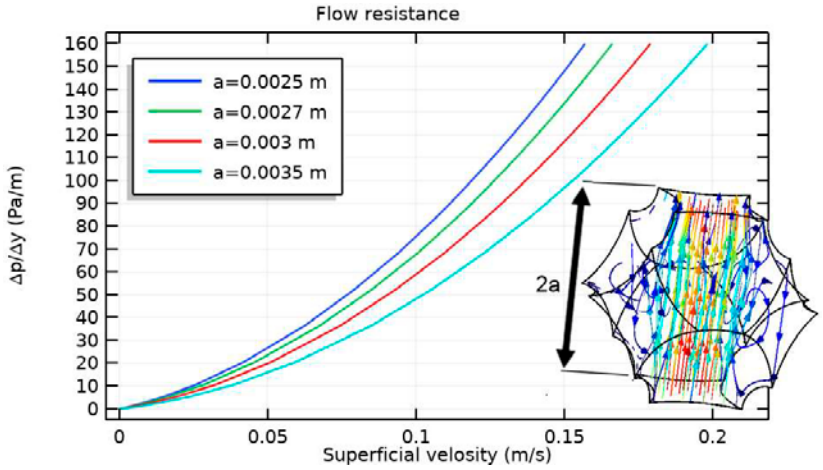

Figure 4-5. *Graph showing the flow resistance over a unit cell with different sizes on the pores in between the pellets.*

5 Mathematical description of the system

5.1 Contact area

Since many of the properties in the model is limited by the contact area between the pellets this area needs to be calculated. The work is based on work that was started in Eriksson (2017) and was initially developed as an attempt quantify the influence of granule size distribution on compaction properties of bentonite clay. However, the model has been improved with a new way of calculating the number of contact points each pellet have with other pellets which mean that the equations can be solved analytically. Since the model was initially intended for compaction and not swelling the volume of the clay is considered constant. This should not affect the result since the result is scalable. The pellet is assumed to be spherical and the geometry is shown in Figure 5-1. This model is dependent on the initial density or porosity of the pellet filling. A lower initial porosity will increase the number of contact points and the area will increase faster.

The contact area can then be calculated with Equations 5-1 and 5-2. Assuming constant volume clay:

$$\frac{4\pi R^3}{3} - \pi n\left(d^2R - \frac{d^3}{3}\right) = \frac{4\pi R_0^3}{3} \qquad \text{Equation 5-1}$$

Where R_0 is the initial radius of the pellets and n is the number of contact points with other pellets. The void space should also be equal the material of the overlapping of the spheres.

$$\pi n\left(d^2R - \frac{d^3}{3}\right) = \frac{\varphi_{a0}-\varphi_a}{1-(\varphi_{a0}-\varphi_a)}\frac{4\pi R_0^3}{3} \qquad \text{Equation 5-2}$$

Where φ_{a0} is the initial inter-granule porosity and φ_a is the inter-granule porosity. These equations should also apply when the inter-pellet porosity is zero and d_m and R_m could be calculated. To calculate the number of contacts, n, the total volume divided with the volume of the cone formed by the contact area as the base and the centre of the sphere as the top at zero porosity, Equation 5-3.

$$n = \frac{4\pi R_m^3}{3\left(\pi\left({d_m}^2R_m - \frac{{d_m}^3}{3}\right) + \pi\left({R_m}^2 - (R_m - d_m)^2\right)(rm - dm)\frac{1}{3}\right)} = \frac{2R_m}{d_m} \qquad \text{Equation 5-3}$$

The equation system above will have the solution according to Equation 5-4 to 5-7.

$$R_m = R_0\left(1 + \frac{\varphi_{a0}}{1-\varphi_{a0}}\right)^{1/3} \qquad \text{Equation 5-4}$$

$$d_m = \frac{3}{2}R_m - \left(\frac{9}{4}{R_m}^2 - 2\,\frac{({R_m}^3 - {R_0}^3)}{R_m}\right)^{1/2} \qquad \text{Equation 5-5}$$

$$R = R_0\left(1 + \frac{(\varphi_{a0}-\varphi_a)}{1-(\varphi_{a0}-\varphi_a)}\right)^{1/3} \qquad \text{Equation 5-6}$$

$$d = R + 2R\cos\left(\pi\frac{2}{3} + \frac{1}{3}\operatorname{atan}\left(\sqrt{3}\,\frac{\sqrt{-3\left(\frac{2d_m}{3R_m}({R^3 - {R_0}^3})\right)^2 + 4\left(\frac{2d_m}{3R_m}({R^3 - {R_0}^3})\right)R^3}}{3\left(\frac{2d_m}{3R_m}({R^3 - {R_0}^3})\right) - 2R^3}\right)\right) \qquad \text{Equation 5-7}$$

The expression derived for the number of contact points can be compared to the unit cells which have known porosity and number of contact points, see Figure 5-2.

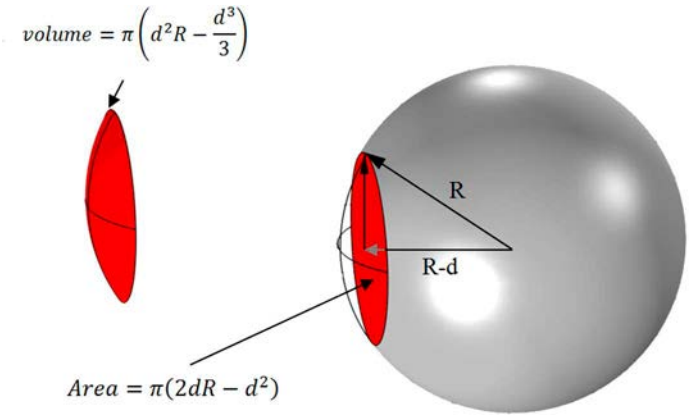

Figure 5-1. *A spherical pellet with the contact area towards another pellet marked in red.*

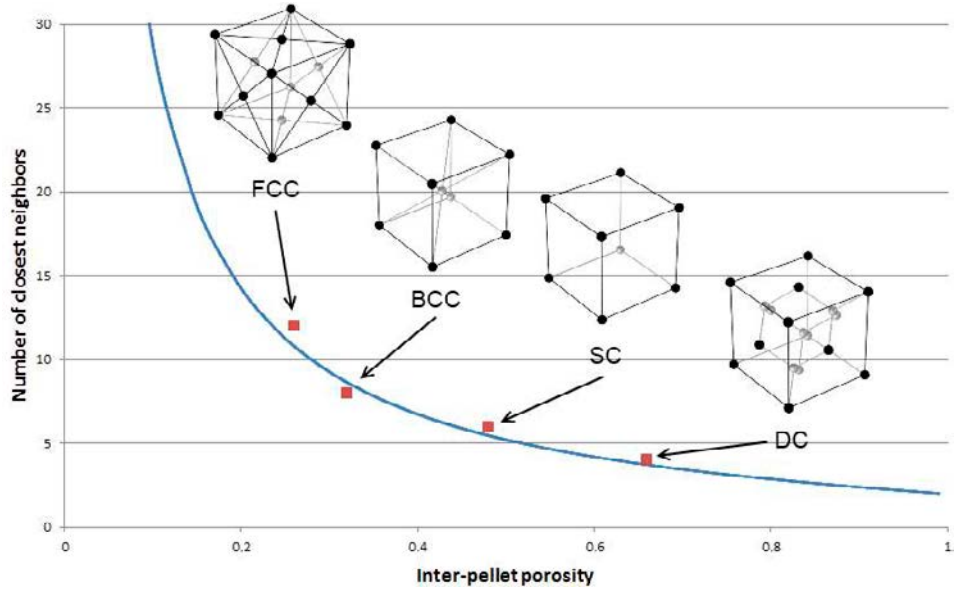

Figure 5-2. *Comparison of the number of closest neighbours between the model and unit cells.*

The normalized contact area between the pellets could then be calculated with Equation 5-8.

$$A_c = \frac{(2dR - d^2)}{(2d_m R_m - {d_m}^2)}$$ Equation 5-8

This expression can then be compared the heat transfer model of the unit cells. If the assumptions are correct then Equation 5-9 should give the similar result, which it does as can be seen in Figure 5-3.

$$\lambda = 1.35A_c$$ Equation 5-9

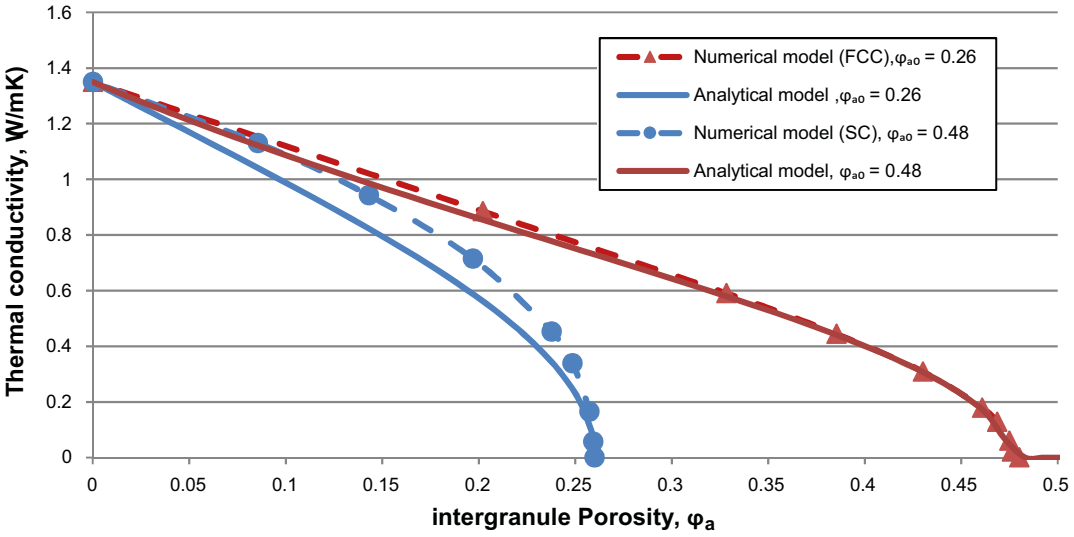

Figure 5-3. *Effective thermal conductivity extracted from numerical modelling of unit cells compared to the analytical model.*

5.2 Suction driven water transport

The water transport in the clay is described with Richard equation, Equation 5-10.

$$\frac{C_m}{\rho_w g}\frac{dp_s}{dt} - \nabla \cdot \left(\rho_w \frac{\kappa}{\mu}\nabla \mathrm{p}_s\right) = Q_m \qquad \text{Equation 5-10}$$

Where C_m is the specific moisture capacity which is defined by Equation 5-11.

$$C_m = \frac{d\theta}{dh} = \rho_w g \frac{d\theta}{dp_s} = g\rho_d \frac{dw}{dp_s} \qquad \text{Equation 5-11}$$

To calculate how the water content changes with suction a retention curve that follows the function in Equation 5-12 is used.

$$w = \frac{a}{(1-RH)} + b\,RH + w_h c_o - (c_o + a) \qquad \text{Equation 5-12}$$

Where RH is the relative humidity which can be recalculated to a suction with Kelvin equation, Equation 5-13, w_h is a function controlling the hysteresis which varies between −1 and 1, w_h is calculated with Equation 5-14.

$$p_s = \frac{RT\rho_w}{M_w}\ln\,(RH) \qquad \text{Equation 5-13}$$

$$w_h = e\int \begin{cases} \frac{dw}{dt} & if\ |w_h| \le 1 \\ 0 & otherwise \end{cases} dt \qquad \text{Equation 5-14}$$

This expression has four fitting constants a, b, c_0 and e. Where a and be controls the shape of the curve c controls how large hysteresis effect there are and e controls how fast the retention curve moves between the drying curve and the wetting curve. The permeability, κ_s, at full saturation is described by Equation 5-15.

$$\kappa_s = A_c \frac{\mu}{\rho_w g} k_1 e^{-k_2 \rho_d} \qquad \text{Equation 5-15}$$

Where k_1 and k_2 are constants, since the pellets are assumed to be saturated this could be recalculated to a function of water content, κ(w), with the Equation 5-16.

$$\rho_d = \frac{1}{\left(\frac{1}{\rho_s} - \frac{w}{\rho_w}\right)}$$ Equation 5-16

The Source term Q_m is used to couple the Richard equation with the diffusion equation and controls the evaporation and condensation of water vapour. This term is described with Equation 5-17. The expression will imply condensation of water if relative humidity in the air is higher than the relative humidity at equilibrium in the clay. R_e is a constant which controls the rate of evaporation/condensation and in this case 0.5 s^{-1} is chosen but it does not affect the model unless a very low value is used.

$$Q_m = -R_e M_w \left(\frac{p_{sv} e^{\left(\frac{p_s M_w}{\rho_w RT}\right)}}{RT} - c \right)$$ Equation 5-17

The saturation pressure of water vapour in the air, p_{sv} (Pa), is described with the Antoine equation, Equation 5-18, M_w is the molar mass of water and c is the vapour concentration of water from the diffusion equation.

$$p_{sv} = 133 \times 10^{\left(8.07131 - \frac{1730.63}{T - 39.724}\right)}$$ Equation 5-18

5.3 Water vapour transport

The vapour transport is modelled with the convection-diffusion equation, Equation 5-19.

Equation 5-19

Where u is the superficial flow velocity of the air moving between the pellets and D_{eff} is the effective diffusion coefficient, described by Equation 5-20. The tortuosity, τ, is the expression found in chapter 4 with the modelling of the unit cells.

$$D_{eff} = \frac{\varphi_a}{\tau} D_v$$ Equation 5-20

Equation 5-21 is used for D_v (m^2/s) (Denny 1993)

$$D_v = 0.187 \times 10^{-9} T^{2.072} \frac{p_o}{p}$$ Equation 5-21

Where p_0 is normal atmospheric pressure.

R_c is the source term which controls evaporation and condensation and it is described by Equation 5-22.

$$R_c = -\frac{Q_m}{M_w}$$ Equation 5-22

5.4 Heat transport

The heat transport is modelled with the heat equation, Equation 5-23.

$$\rho C_p \frac{dT}{dt} + \rho C_p u \cdot \nabla T - \nabla(\lambda \nabla T) = 0 \qquad \text{Equation 5-23}$$

The thermal conductivity is assumed to be dependent on the contact area between the pellets. The thermal conductivity of the individual pellets is assumed to have a thermal conductivity of saturated bentonite. Therefore the thermal conductivity of the pellets is assumed to be the contact area multiplied with the saturated thermal conductivity. However, since the contact area is close to zero when no swelling has occurred this would imply a thermal conductivity of zero. To get a more reasonable model is also assumed that heat can be transferred in the air between the pellets. The thermal conductivity in the pellets and the thermal conductivity can be added by assuming that the heat flow takes place parallel to each other. The result of this is shown in Equation 5-24.

$$\lambda = \lambda_s A_c + \lambda_{air} \frac{(1-A_c)^2}{\varphi_a} f_g \qquad \text{Equation 5-24}$$

Where f_g is a geometric factor which would change if the pellet geometry changes. For the case of spherical pellets a value of 3 is used. λ_s is the saturated thermal conductivity and λ_{air} is the thermal conductivity of air, in this case 0.02 is used. The analytical expression is compared to the results for the numerical modelling on unit cells in Figure 5-4.

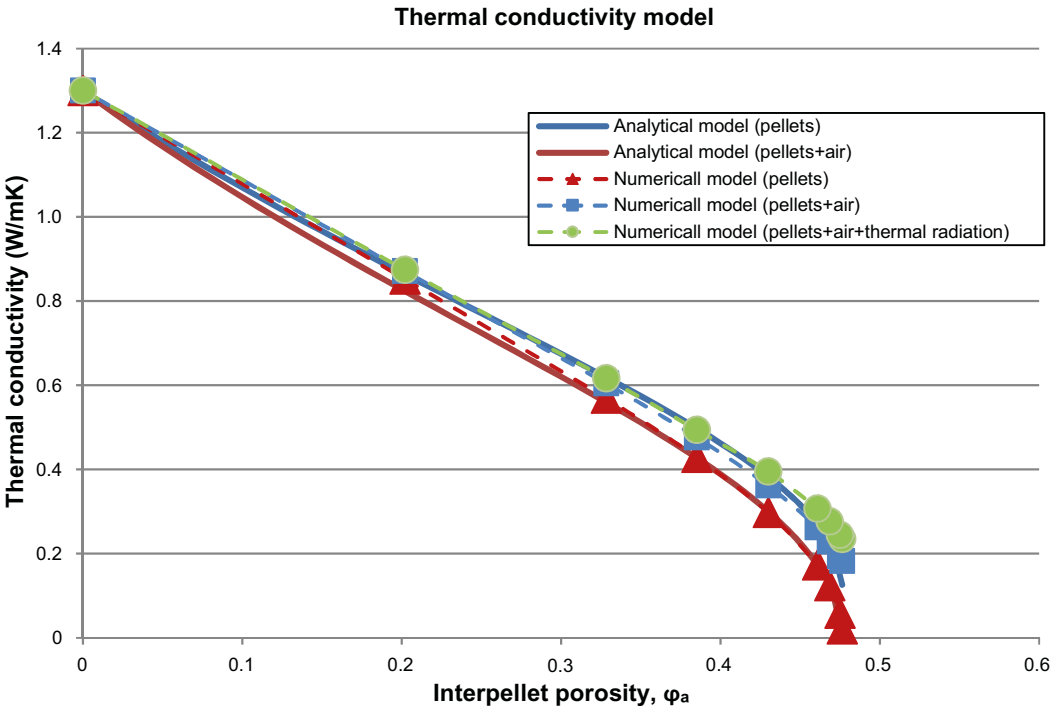

Figure 5-4. *Analytical thermal conductivity model compared to thermal conductivity calculated from numerical modelling of unit cells.*

5.5 Fluid flow

Since the vapour transport is influenced by the air flow this air flow needs to be modelled. The flow in the pores are calculated with Navier-Stokes equation when only air is present and in the case where a two-phase flow (air and water) is present in the pores a two-phase Darcy flow is used. But since the pellets will restrict the flow the flow resistance needs to be estimated. To do this the Ergun equation is used, Equation 5-25.

$$\frac{dp}{dx} = c_l \frac{v_s \mu \ (1-\varphi_a)^2}{4 r_0^2 \varphi_a^3} + c_t \frac{\rho v_s^2 (1-\varphi_a)}{2 r_0 \varphi_a^3}$$ Equation 5-25

This equation suggests that the flow resistance is dependent on inter-pellet porosity, the size of the pores and the flow velocity. The Ergun equation is compared to the results from the modelling of the unit cell and this shows that the equation gives a rather good agreement, see Figure 5-5.

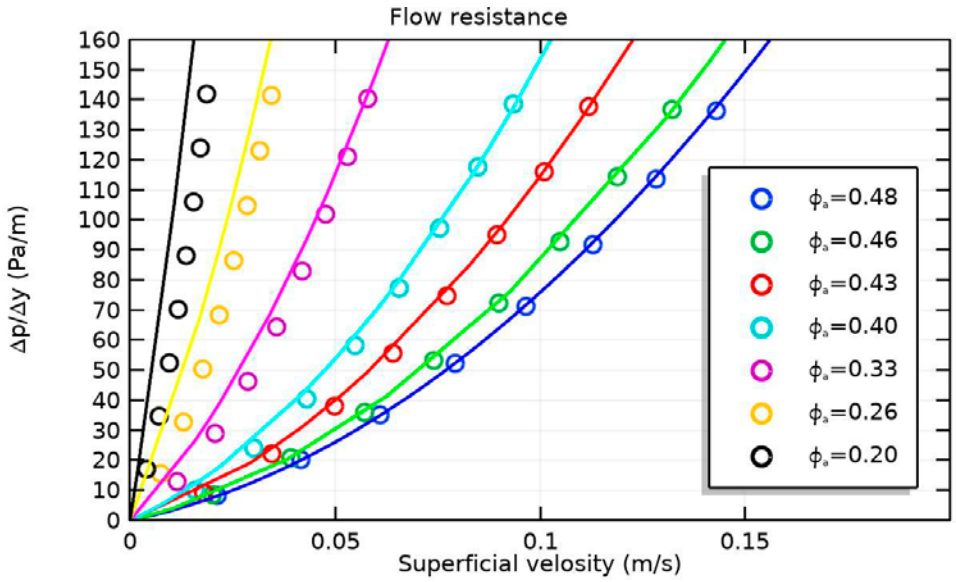

Figure 5-5. *Flow resistance from numerical modelling (circles) compared to Ergun equation (solid lines).*

6 Data and material specific input to the model

6.1 Hydraulic conductivity

In the model the hydraulic conductivity or the permeability of the material is needed to describe transport of liquid water. This parameter has been measured for both of the materials (TR-16-04). MX-80 material has lower hydraulic conductivity then the Asha material. The materials in the test has been converted to a calcium bentonite before the final density was measured, therefore the measured dry densities is slightly too high. This is because the calcium chloride goes in to the bentonite and adds extra weight the test sample. The original dry density values which would represent the density with deionized water can be calculated by taking the mass of the salt in account. The recalculated data can then be compared to swelling pressure tests performed with deionized water. The process of recalculating the data is described further in Svensson et al. (2017).

The saturated hydraulic conductivity, K_s, can be described by an exponential function as described in Equation 6-1. The constants k_1 and k_2 are material specific and shown in Table 6-1.

$$K_s = k_1 e^{-k_2 \rho_d} \qquad \text{Equation 6-1}$$

The results and the relation used in the model for the Asha clay and MX-80 is shown in Figure 6-1.

Table 6-2. Constants used in Equation 6-1 to describe hydraulic conductivity.

Material	k_1 (m/s)	k_2 (m^3/kg)
Asha	4e−10	0.0051
MX80	3e−10	0.0055

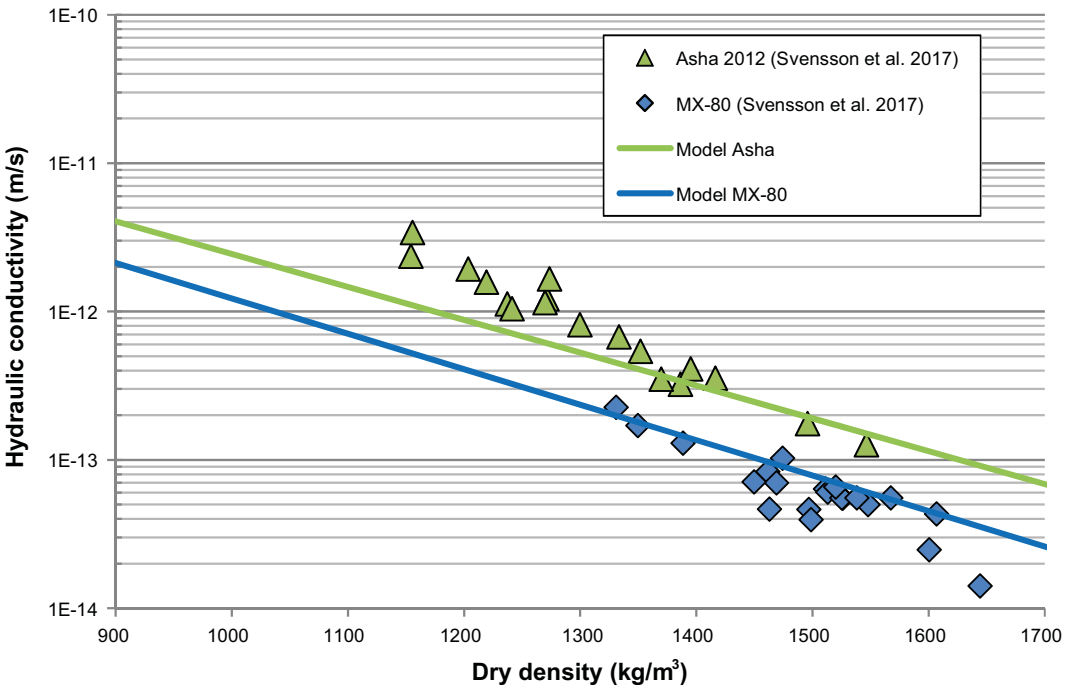

Figure 6-1. *Hydraulic conductivity models compared to data.*

As described in chapter 3 and 4 the transportation properties are assumed to be limited by the contact area between the pellets. Therefore, the expression for the total hydraulic conductivity of the pellet filling can be described by multiplying the saturated hydraulic conductivity with the contact area between the pellets according to Equation 6-2.

$$K(w) = \frac{\mu}{\rho_w g}\kappa(w)A_c \qquad \text{Equation 6-2}$$

If the permeability is divided with the permeability at full saturation, κ_s, and compared to a relative permeability with a power law of saturation, Equation 6-3, it can be seen in Figure 6-2 that the two expressions would be almost the same if an exponent, ξ, of 5 is used as a relative permeability.

$$\kappa_{r1} = S_r{}^{\xi} \qquad \text{Equation 6-3}$$

$$\kappa_{r2} = \frac{\kappa(w)A_c}{\kappa(w_{sat})} \qquad \text{Equation 6-4}$$

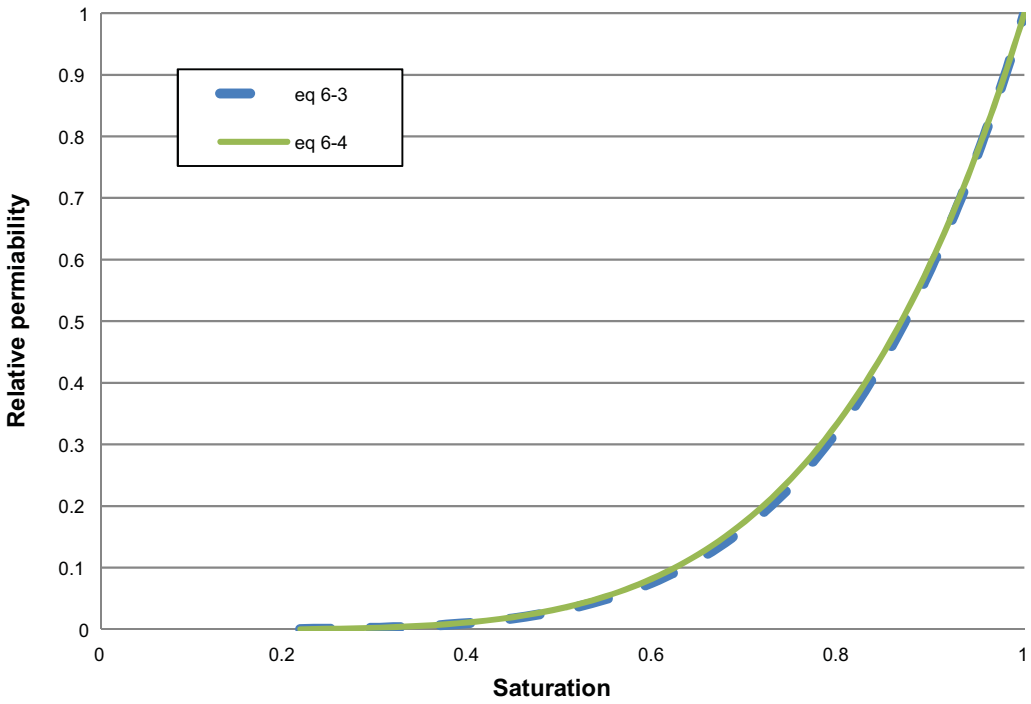

Figure 6-2. *Equation 6-3 and Equation 6-4 compared to each other.*

6.2 Retention properties

Since there are limited amount of data on the retention properties on the Asha material the retention properties is fitted against swelling pressure data from Svensson et al. (2017). The swelling pressure is recalculated to a relative humidity with the Kelvin equation.

Using the constants found in Table 6-2 the curve can be compared to the data for Asha with is shown in Figure 6-5 and in greater detail at high RH in Figure 6-6. The results suggest that this retention curve works quite well for water contents below approximately 40 %. However, for higher water contents the curve seems to overestimate suction.

Table 6-2. Constants used in Equation 5-12 to describe the retention curve.

Material	a	b	c_o	e
Asha	0.002	0.32	0.035	0.03
MX80	0.003	0.29	0.035	0.03

For MX-80 there are more data available and in Figure 6-3 Equation 5-12 is plotted with the constants a, b, c and e from Table 6-2 and in greater detail at high RH in Figure 6-4. The same is done for the Asha material in Figure 6-5 and 6-6.

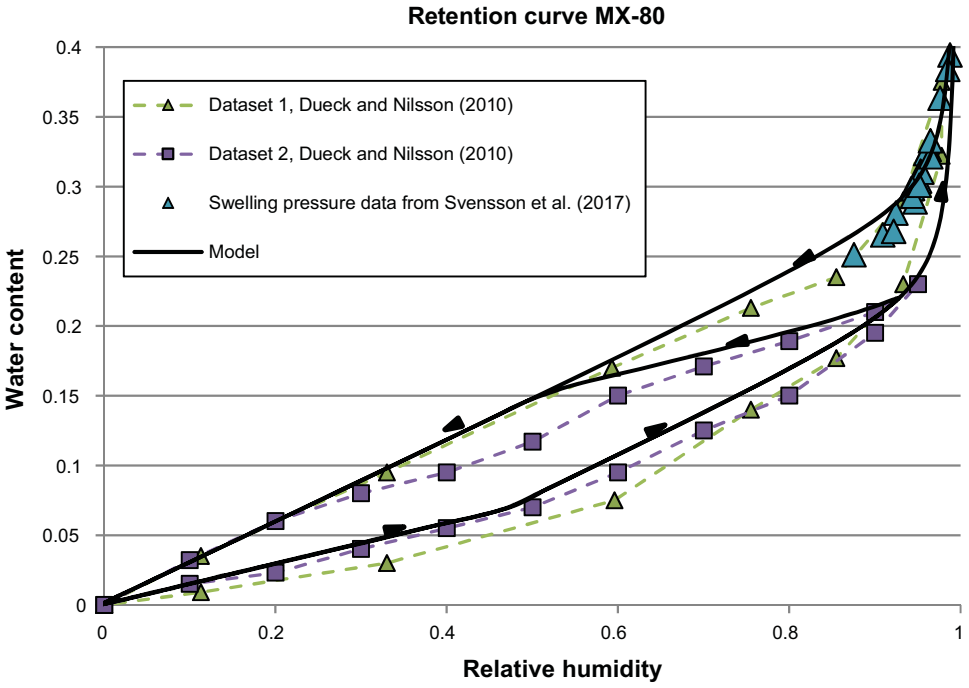

Figure 6-3. *Retention curve used for MX80. Swelling pressure data is recalculated with the Kelvin equation to a relative humidity.*

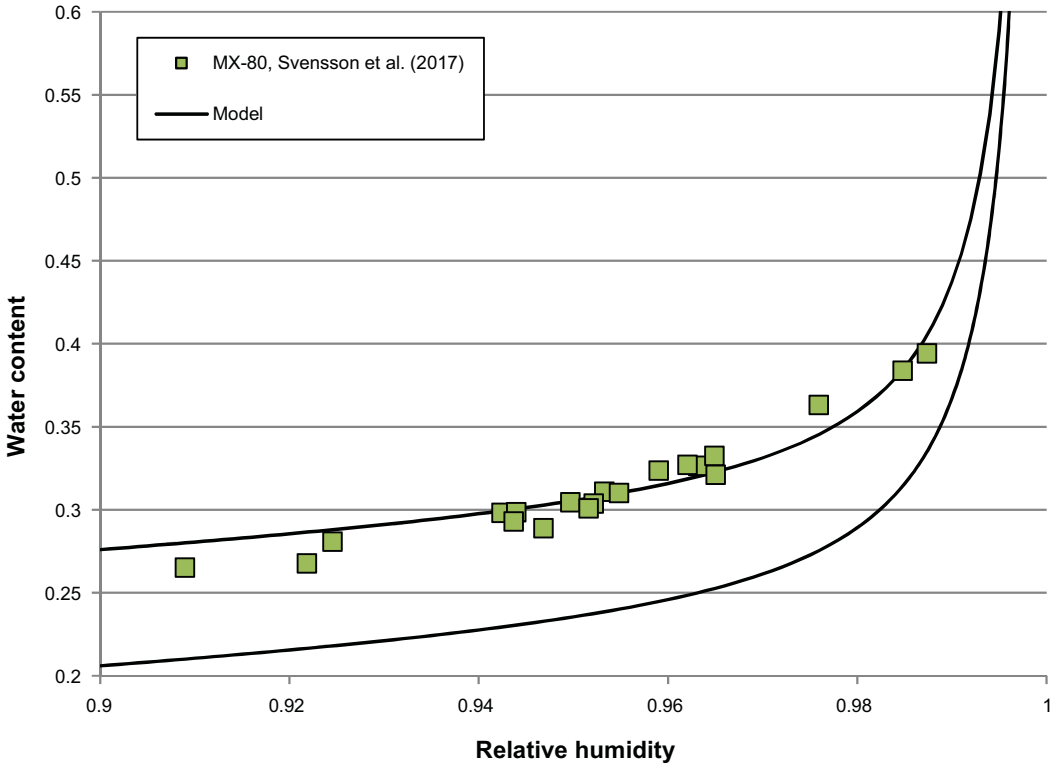

Figure 6-4. *Retention curve used for MX80 at high relative humidity. The data is swelling pressure recalculated with the Kelvin equation to a relative humidity.*

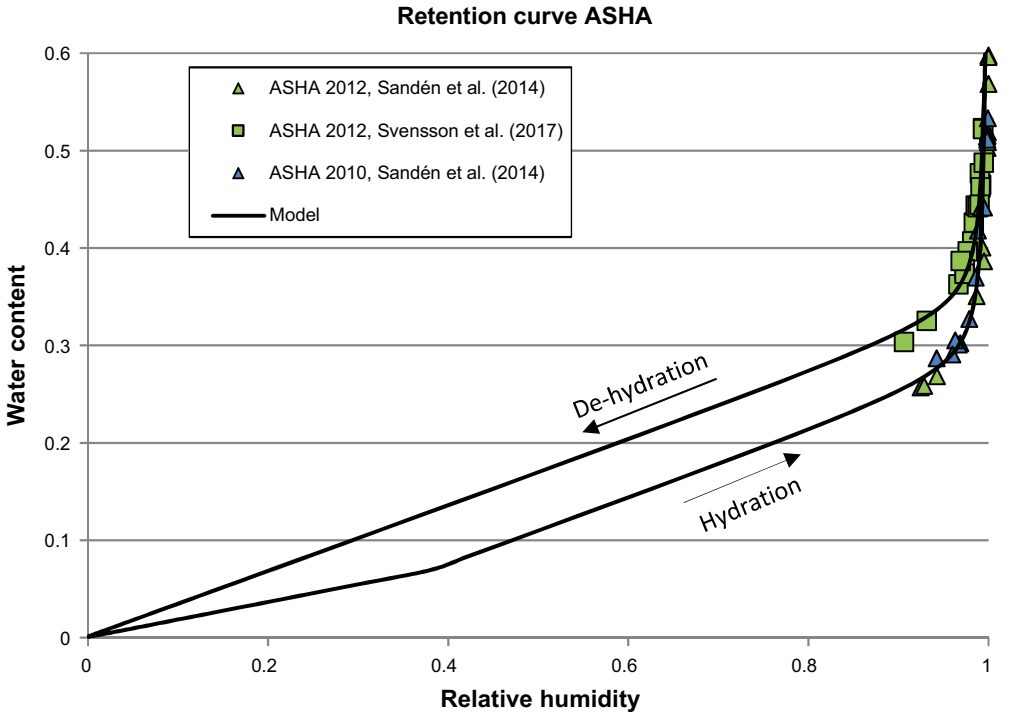

Figure 6-5. *Retention curve used for Asha. Data from Svensson et al. and Sandén et al. is swelling pressure data which is recalculated with the Kelvin equation to a relative humidity.*

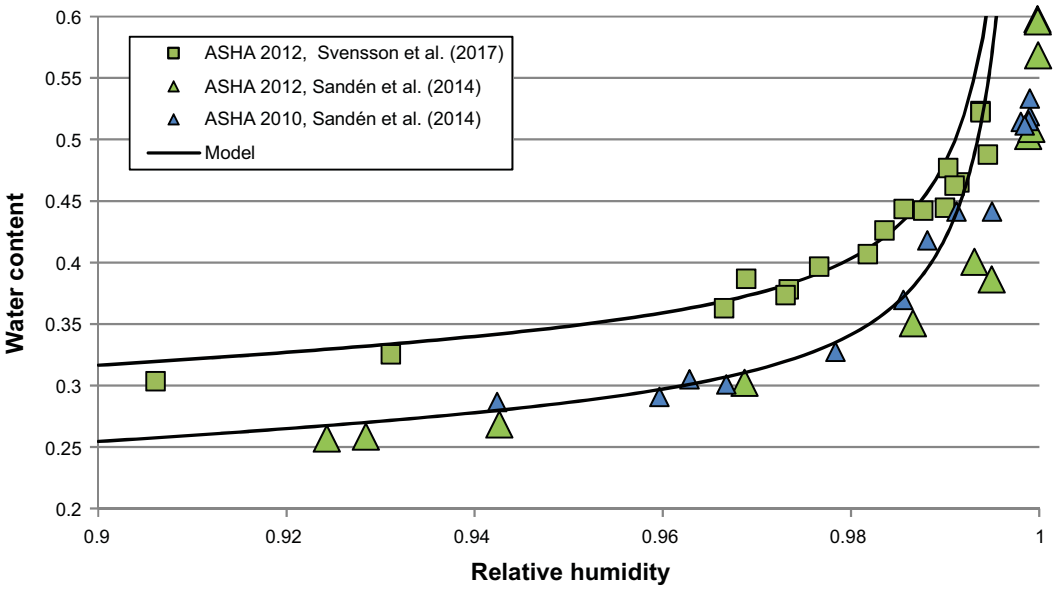

Figure 6-6. *Retention curve used for Asha at high relative humidity. Data from Svensson et al. and Sandén et al. is swelling pressure data which is recalculated with the Kelvin equation to a relative humidity.*

6.3 Thermal conductivity

Not many thermal conductivity measurements on pellet fillings have been found to calibrate the models. Therefore measurements on compacted bentonite are used which is taken from Svensson et al. (2019). The granular material could be considered as small pellets that have been compacted and then be compared to the model, Figure 6-7. A initial inter-granule porosity of 0.4 was chosen for MX80 which correspond to an initial (before compaction) dry density of 1 140 kg/m^3 with a water content of 17 %,

The saturated thermal conductivity, λ_s, is then approximately 1.35 W/mK for MX80 and 1,23 W/mK for the Asha material.

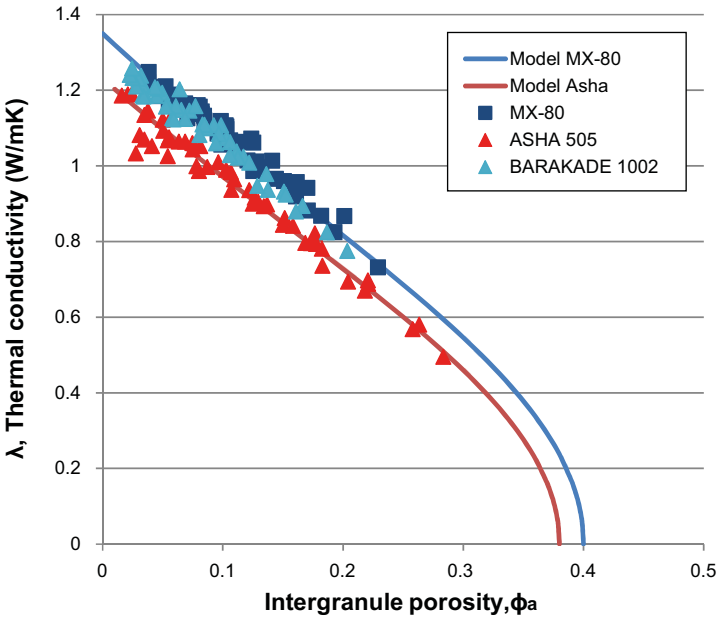

Figure 6-7. *Thermal conductivity model compared to data on compacted bentonite from Svensson et al (2019). BARA-KADE material is added as comparison as it very similar to MX80.*

6.4 Flow resistance

The Ergun equation is calibrated against flow resistance data (Luterkort et al. 2017) that has been measured for roller compacted pellets for two different dry densities. By using the parameter values given in Table 6-3 the Ergun equation fits rather well, see Figure 6-8.

Table 6-3. Parameters used in the Ergun equation (Equation 5-25)

c_l (1)	c_t (1)	r_0 (m)
150	4	0.00245

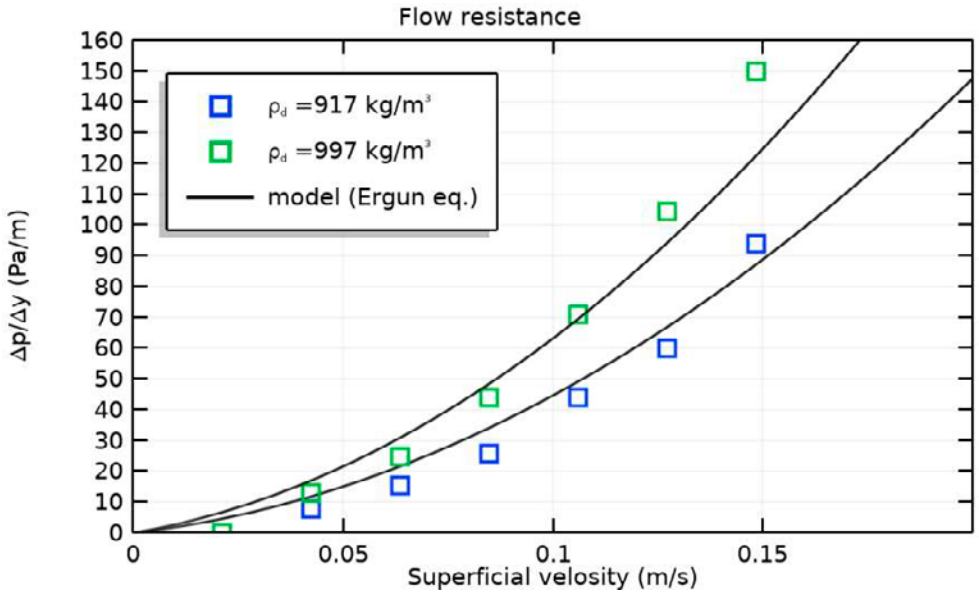

Figure 6-8. *Ergun equation compared to data from Luterkort et al. (2017)*

7 Modelling and validation

7.1 Validation cases

Three different tests are used to test the model. Two of them have been performed within the EBS task force, Task 10 subtask A and Task 10 subtask C. Task 10 subtask A is designed to test the suction driven transport whereas Task 10 subtask C is designed to test the transport of water vapour when a thermal gradient is present. The third test used is a test in which higher water inflows is added to a pellet filling to get free water moving in between the pellets. This test was performed at Äspö HRL in 2018.

7.2 Task 10 subtask A

7.2.1 Description of test

This test is performed in an acrylic glass tube with a height of 50 cm and a diameter of 10 cm filled with pellets. A water inlet is placed on the bottom of the tube where the water is added at constant pressure. Relative humidity is measured in three places, 3, 8 and 15.5 cm from the bottom in the test Ar3. Water consumption is measured in all the tests and after the termination of the test water content is measured as a function of height. The test setup is shown in Figure 7-1. The test matrix is shown in Table 7-1.

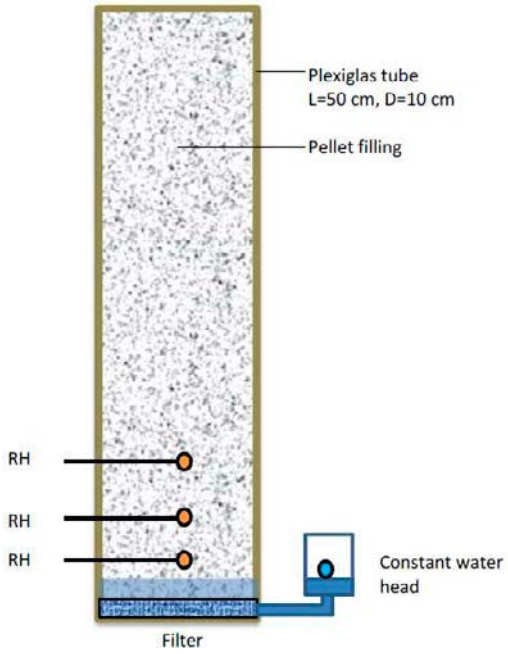

Figure 7-1. *Test setup*

Table 7-1 Test matrix

Test	Pellet type	Material	Duration	Inlet pressure	Measurements
Ar1	Roller compacted	MX80	5 days	0.1 kPa	Water consumption Water content
Ar2	Roller compacted	MX80	30 days	0.2 kPa	Water consumption Water content
Ar3	Roller compacted	MX80	203 days	1 kPa	Water consumption Water content Relative humidity
Ae1	Extruded	Asha	5 days	0.2 kPa	Water consumption Water content
Ae2	Extruded	Asha	30 days	0.2 kPa	Water consumption Water content
Ae3	Extruded	Asha	202 days	1 kPa	Water consumption Water content

7.2.2 Boundary and initial conditions

The volume is assumed to be constant which means that no displacement of pellets will take place. All the boundaries are considered closed for water and vapour except the lower boundary where a fixed pressure of zero Pa is applied. In this model there is also an assumption made that no water will be transported as free water in the pore space. The initial water content is set to 14.7 %.

7.2.3 Result roller compacted pellets

The modelled water content has a good agreement with the measured, see Figure 7-2. Modelling has been done both with vapour diffusion included and without. In the model almost all of the vapour transport below a water content of approximately 20 % is by diffusion. Therefore, diffusion needs to be considered to get a good result. Also the relative humidity is well replicated with some small deviation at the height 15.5 cm, see Figure 7-3.

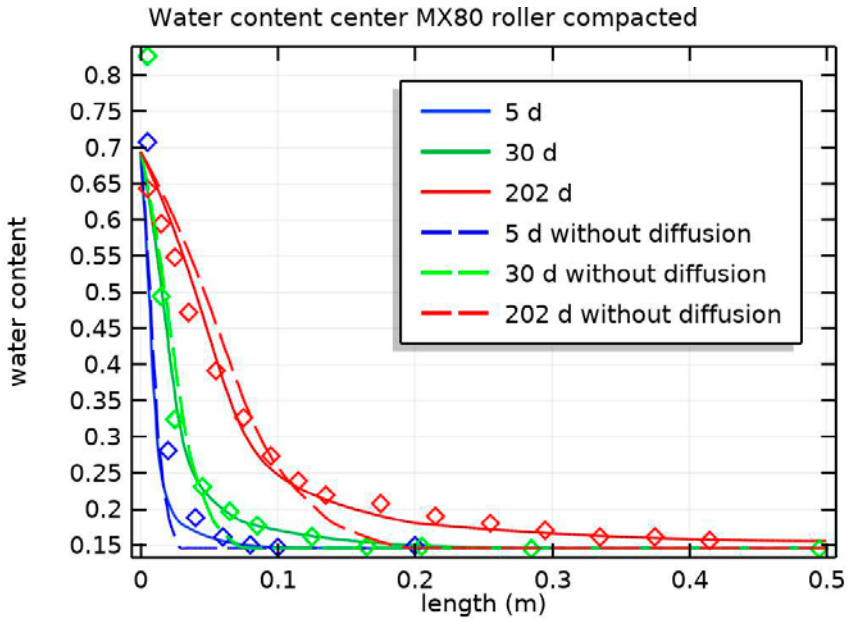

Figure 7-2. *Modelled result (lines) compared with test (diamonds) for the water content with the roller compacted pellets.*

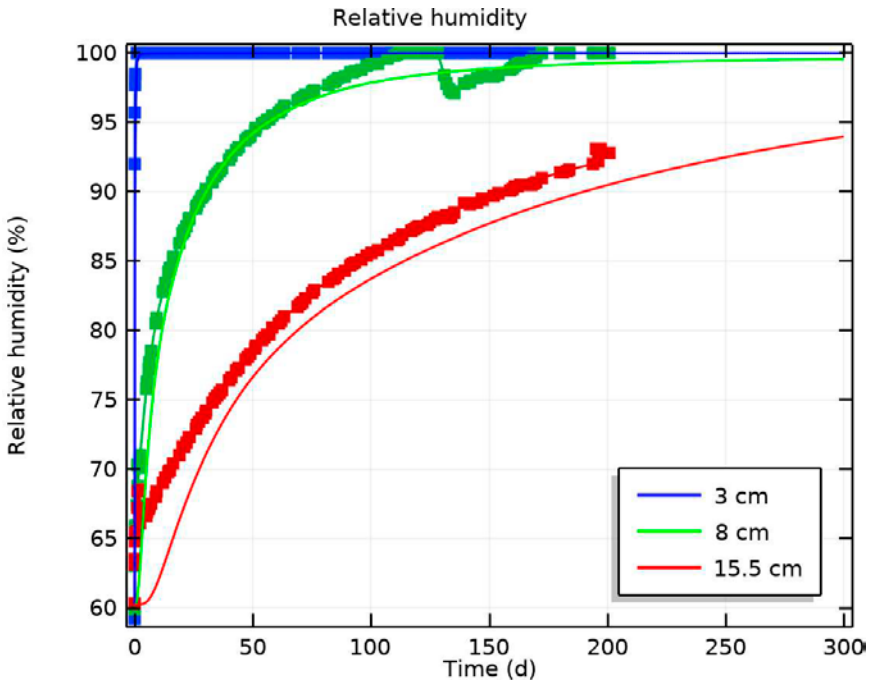

Figure 7-3. *Modelled result (lines) compared with test (squares) for the relative humidity on roller compacted pellets.*

From water uptake data it seems like a lot of water is absorbed during the first hours. However, if the amount of water is absorbed in the test is calculated by integrating the water content over the volume then it can be concluded that this first phase is mainly filling up tubes and filters with water. Although there could also be some water filling up in the bottom of the test in the early stage. Therefore it should be valid to remove the water consumed during this first phase to get a better comparison between the data and the model, Figure 7-4. The result has a rather good agreement as expected when the water content also have a good agreement.

7.2.4 Result extruded pellets

Results for the extruded also shows a good fit with data. No major differences between the models for the extruded and the roller compacted pellets are present. The differences between the two models are related to material parameters like retention properties and hydraulic conductivity due to that they are made of different materials. The modelling results are compared to data in Figure 7-5 and Figure 7-6.

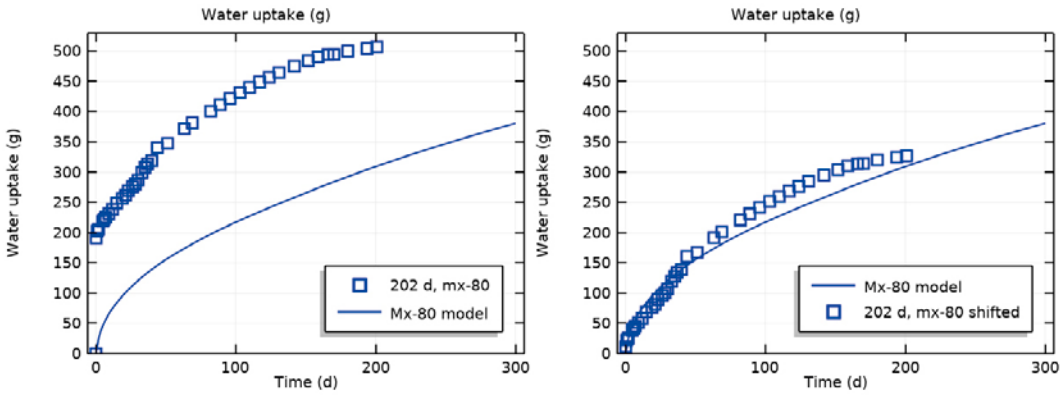

Figure 7-4. *Modelled result (lines) compared with test (diamonds) for the water inflow for roller compacted pellets. Left graph is measured data and right graph the initial water consumption is removed.*

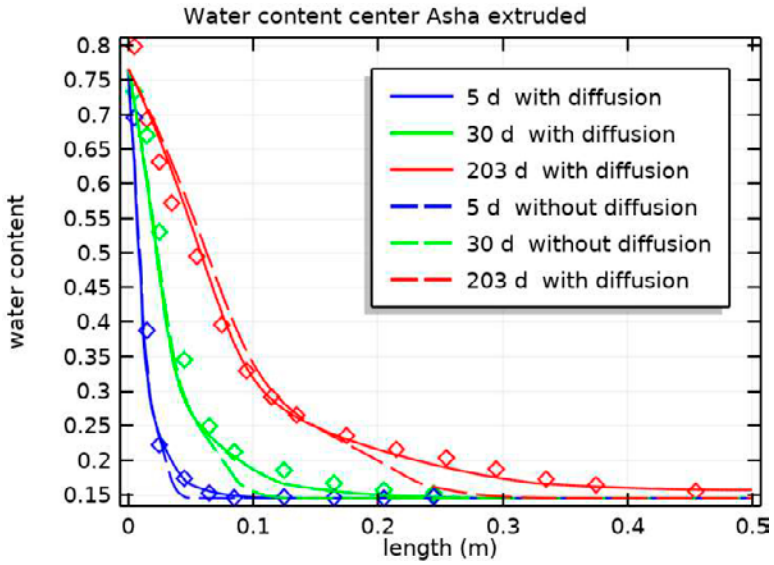

Figure 7-5. Modelled result (lines) compared with test (diamonds) for the water content with the extruded pellets.

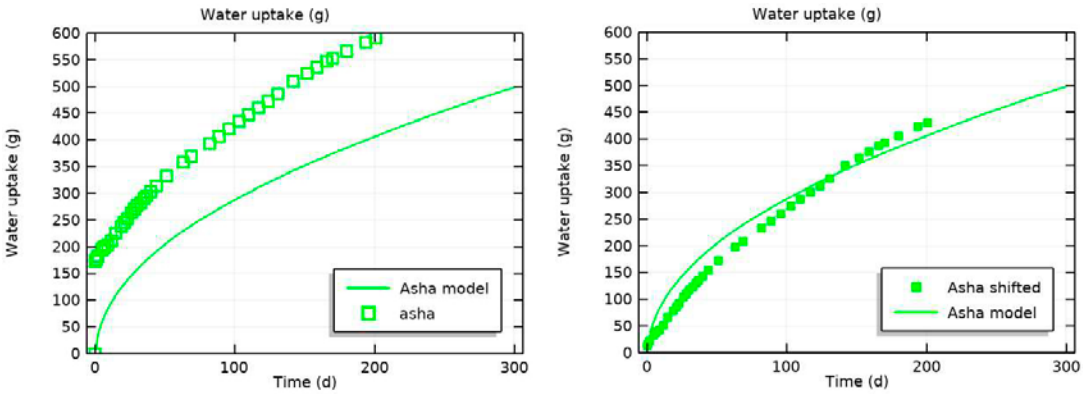

Figure 7-6. Modelled result (lines) compared with test (diamonds) for the water inflow for extruded pellets. Left graph is measured data and right graph the initial water consumption is removed.

7.3 Task 10 subtask C

7.3.1 Description of test

Test setup is shown in Figure 7-7. it is performed in a 50 cm high acrylic glass tube with a diameter of 10 cm. The tube is sealed in the ends and a temperature gradient is applied over the test in vertical direction. Isolation is placed on the outer surfaces and RH measurements are performed a 5 places and the temperature measurements are performed at 7 places. After the termination of the test water content is measured along the height of the test. The test matrix is shown in Table 7-2.

Table 7-2 Test matrix for task 10 C

Test	Pellet type	Material	T_h/T_c	Duration	Measured
CR1	Roller compacted	MX80	74/24°C	5 h	T, w
CR3b	Roller compacted	MX80	74/24°C	7 days	T, RH, w
CR3c	Roller compacted	MX80	74/24°C	14 days	T, w
CR3d	Roller compacted	MX80	74/24°C	90 days	T, RH, w
CR3e	Roller compacted	MX80	74/24°C	365 days	T, RH, w
Ce3d	Extruded	MX80	74/24°C	90 days	T, RH, w

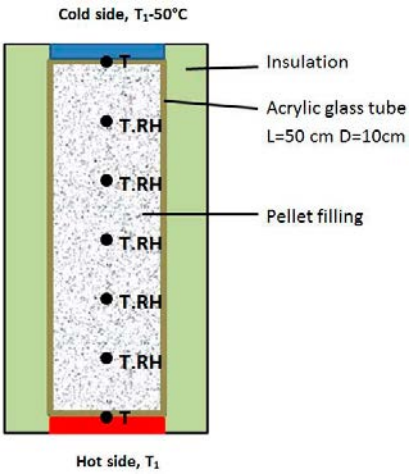

Figure 7-7. Test setup

7.3.2 Boundary and initial conditions

Since no water is added or removed from the test it is assumed that the inter-pellet porosity is constant. This is because all the pellets are considered to be saturated and as the drying pellets shrinks the ones with increasing water content expands. Therefore the pellet filling is moving downwards as the pellets dries in the bottom. In reality the pellets are not saturated and swelling and shrinkage is not linear with water content. Because the inter-pellet porosity does not change this also mean that the thermal conductivity in the model will be constant. The initial water content is set to 14.5 % and the starting place in the retention curve is set to fulfil the relative humidity measured in the beginning of the test.

All boundaries are set as sealed for water transport. A constant temperature boundary condition is set on the top and the bottom. The temperature in the bottom is set to 74°C and in the top to 24°C. On the side boundaries a heat transfer coefficient of 0.15 W/(m^2°C) is used.

7.3.3 Result roller compacted pellets

The water content, shown in Figure 7-8, shows mostly a good agreement with the data. However, the water content in the top is underestimated for the 90 day test, the reason for this in not clear. The Relative humidity is shown in Figure 7-9 and captures the trends but is underestimated for the values close to the bottom where the highest temperatures were observed. It is likely that this can be improved by adding a temperature dependence on the suction which would decrease the suction as the temperature increases. The temperature seems to be captured well, Figure 7-10. The displacement of the pellets can be calculated from the water content distribution with Equation 7-1 and is compared to measurements in Figure 7-11. The result suggests that the assumption that the inter-pellet porosity is constant is not completely correct and it suggests that some reduction in inter-pellet porosity takes place in the upper half of the test.

$$d_{disp}(z) = \int_0^z V_w(\dot{z}) - V_{w,initial} d\dot{z} = \int_0^z \theta(\dot{z}) - \theta_{initial} d\dot{z} \qquad \text{Equation 7-1}$$

Where V_w is the volume of water.

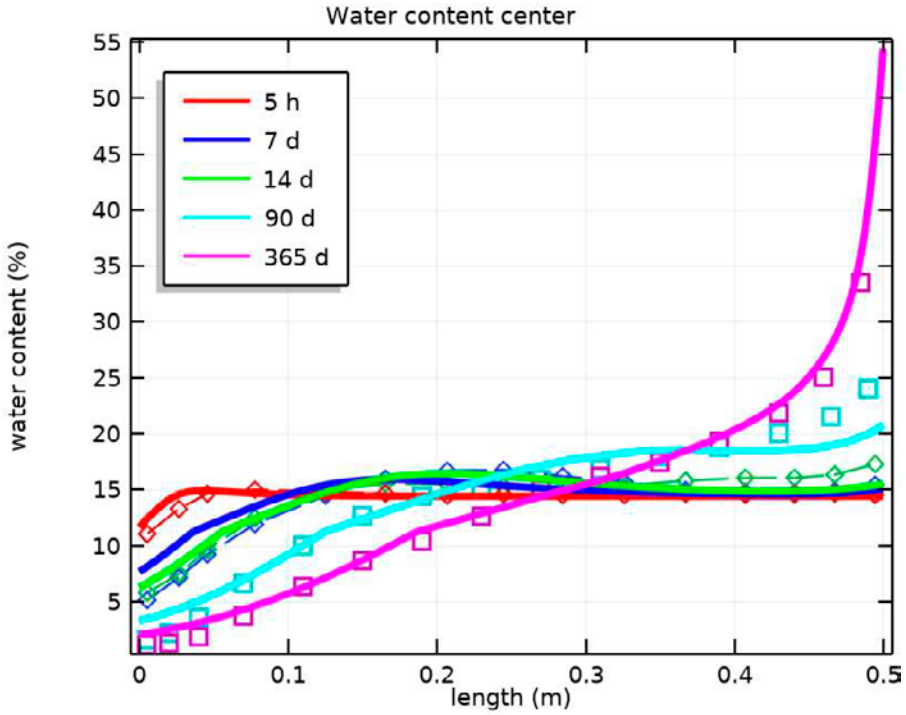

Figure 7-8. *Modelled water content (solid lines) compared to test result for roller compacted pellets.*

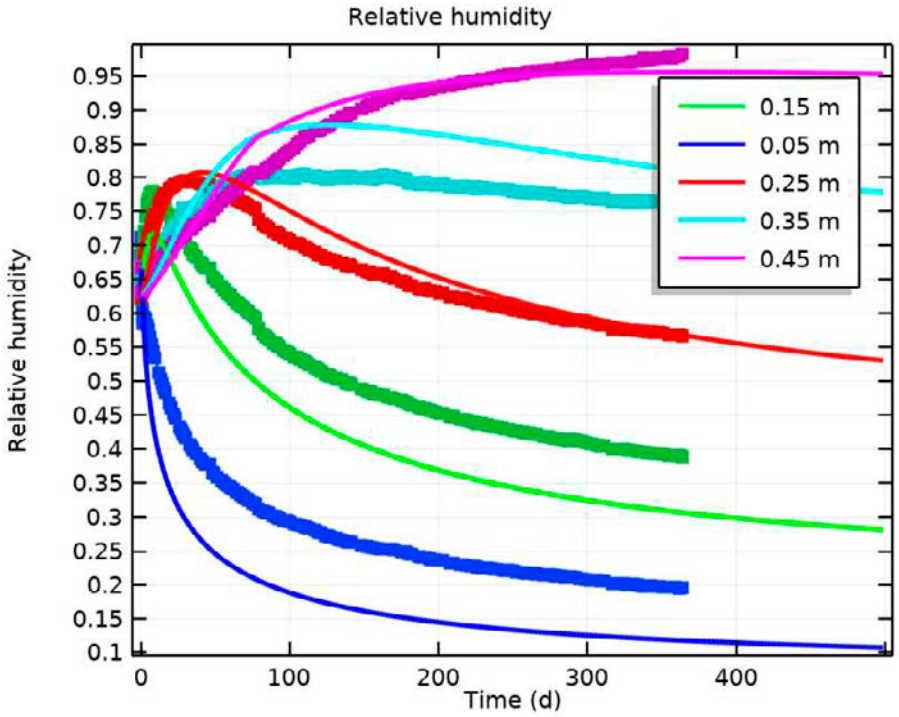

Figure 7-9. *Modelled relative humidity (solid lines) compared to test result for roller compacted pellets.*

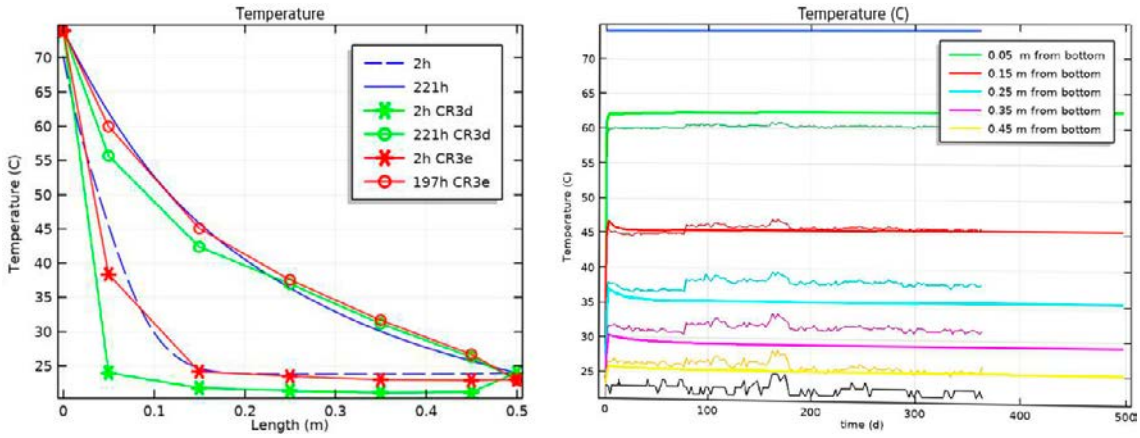

Figure 7-10. *Left figure modelled Temperature (blue lines) compared to test result for roller compacted pellets. Right figure shows the Temperature as a function of time compared to the sensors.*

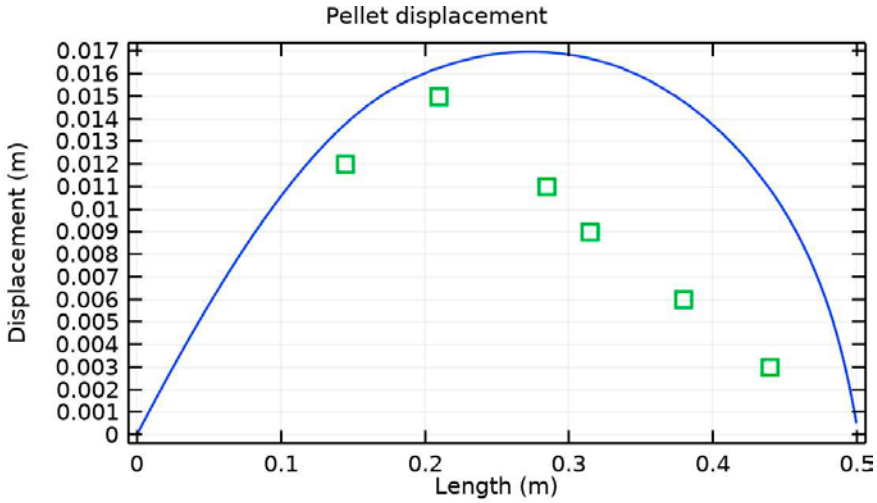

Figure 7-11. *Modelled pellet displacement (solid lines) compared to test result for roller compacted pellets.*

7.3.4 Result extruded pellets

The comparison between the data and the modelling result are shown in Figure 7-12 to Figure 7-14. The result is very similar to that of the roller compacted pellets. The model underpredicts the water content in the top of the test and the relative humidity at the hotter parts of the test. The reason for this is likely related to that the retention curve used in this model is not completely correct. The temperature is however, well captured.

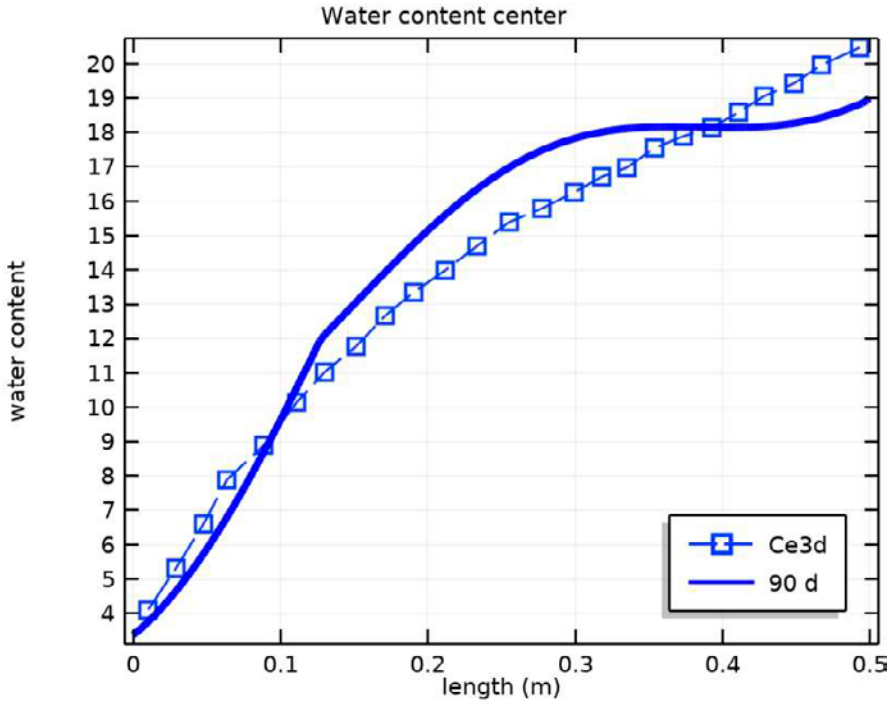

Figure 7-12. *Modelled water content (solid lines) compared to test result for extruded pellets.*

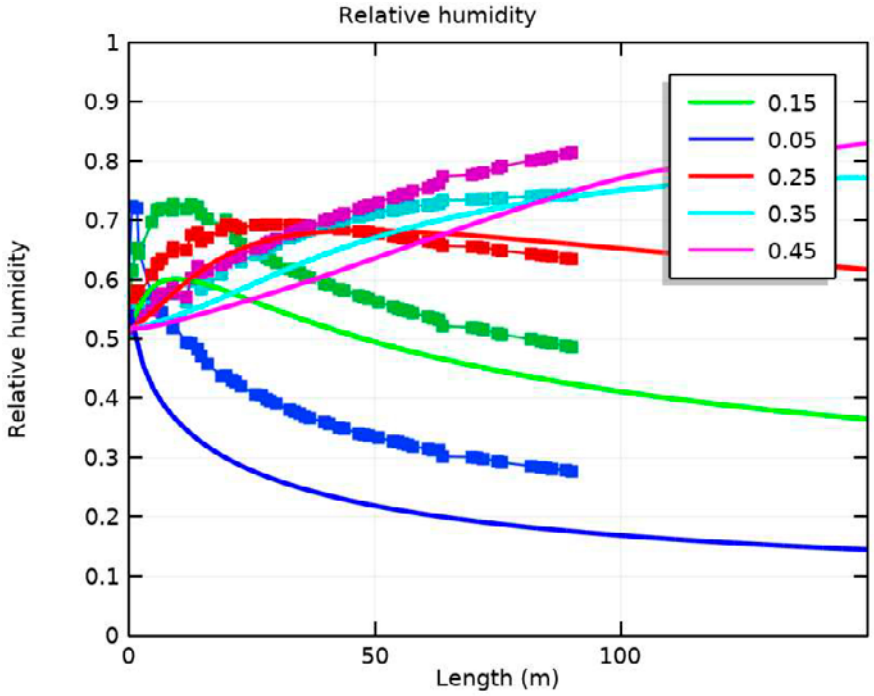

Figure 7-13. *Modelled relative humidity (solid lines) compared to test result for extruded pellets*

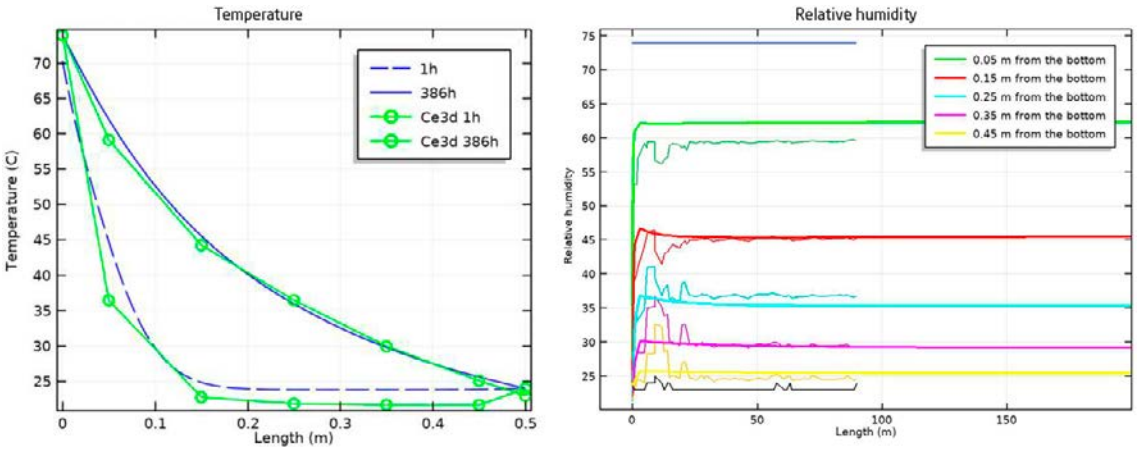

Figure 7-14. *Left figure: modelled Temperature (blue line) compared to test result for extruded pellets. Right figure shows the Temperature as a function of time compared to the sensors.*

7.4 Modelling of free water in between the pellets.

7.4.1 Description of test

To test the models capability of predicting a higher inflow of water which will be transported in between the pellets a test carried out at Äspö HRL is used to compare the model with data. These tests consist of a rectangular box according to the dimensions shown in Figure 7-15. The box is filled with pellets and water is pumped in at a constant rate. The wetting process is captured with a camera and the water pressure at the inlet is measured. More details about the test can be found in Lundgren and Johannesson (2019). The inflow has been varied for different tests but in this work focus has been on roller compacted pellets of BARA-KADE with inflows of 0.1 l/min and 0.01 l/min. BARA-KADE is a clay from Wyoming is very similar to MX80, and these two inflow rates have been chosen because they show two totally different behaviour. At the higher inflow, 0.1 l/min the water flows to ha bottom and fills the test setup from the bottom up. At the lower inflow 0.01 l/min the inflow is more symmetric.

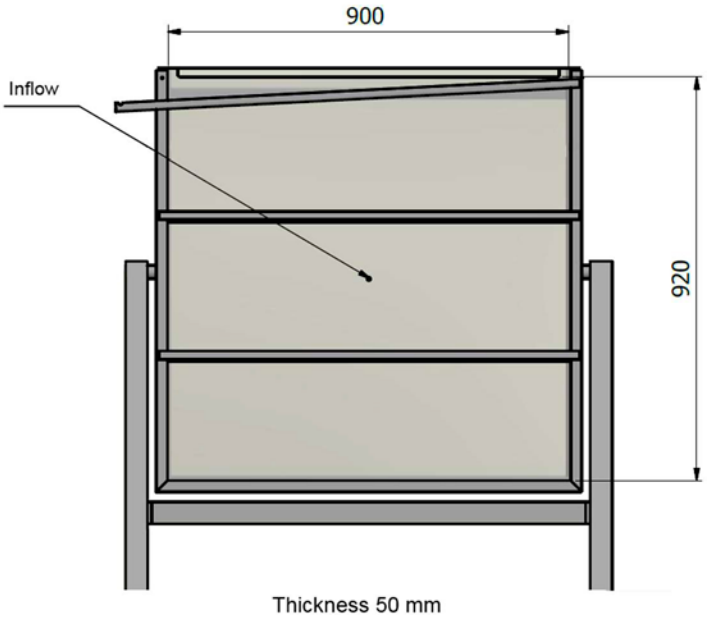

Figure 7-15. *Dimension of the test.*

7.4.2 Modelling

To do the modelling the equations described in chapter 5 is used with the flow in between the pellets are modelled as a two-phase Darcy flow. A capillary pressure model by Corey and Brooks is used with an entry capillary pressure of 1.3 kPa. The entry capillary pressure is set to a rather high number to get good convergence. However, the rather high value gives a larger spreading in horizontal direction at high flows. Darcy flow does not have velocity dependence in the flow resistance which the data shows that the pellet fillings have. Therefore only the linear term in the Ergun equation is recalculated to permeability. This means that the flow rate should only be valid for low flows. In the model a 2D square is used which has the side 1m which is not exactly the same as the test. This shows in the higher inflow rate as the water level is a little bit lower than in the test. The absorption rate in kg/(m^{3}s) is assumed to be proportional to the average suction according to Equation 7-2.

$$R_{absorp} = 12 \times 10^{-8} p_s \qquad \text{Equation 7-2}$$

7.4.3 Results 0.01 l/min

The model predicts that the water will start to flow downwards but as the pellets swell the water will start to spread to the sides. After a while the flow turns upwards as the pellets swells and seals up in the first wetted areas. The modelled result can be seen compared to the test in Figure 7-16.

The model starts to have convergence problems at approximately 4 h due to that the pellets seals up and the pressure increases fast, see Figure 7-17. If the pressure evolution is compared to that from the test, Figure 7-18, it follows the pressure reasonable up to approximately up to 3 hours in to the simulation. After that pressure peaks start to appear in the test data indication that pipes are formed in the pellet filling. Since this piping phenomenon is not captured in the current model the result should only be valid up to this point.

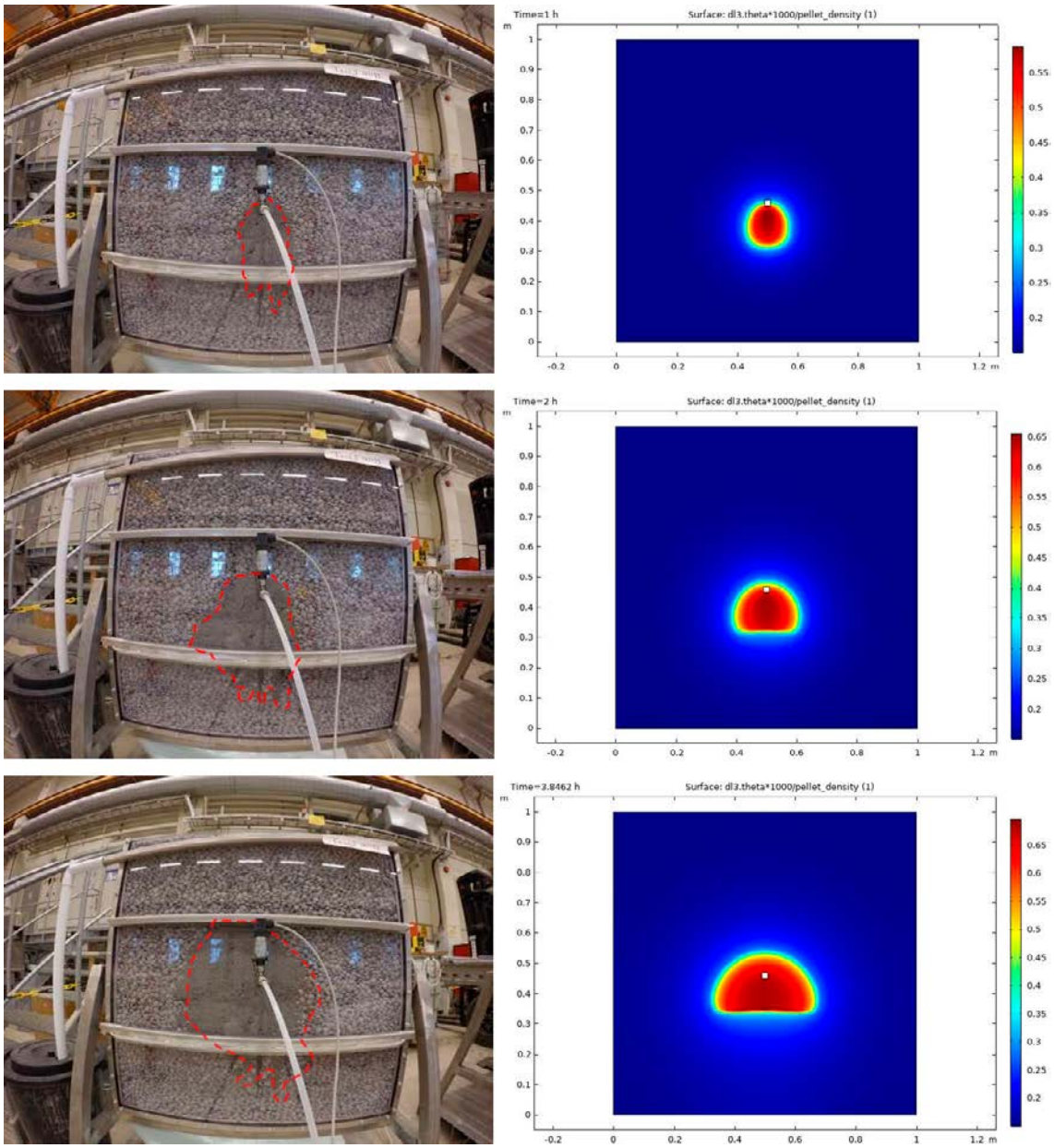

Figure 7-16. *Wetting comparison between the test and the model after 1, 2 and 4 hours.*

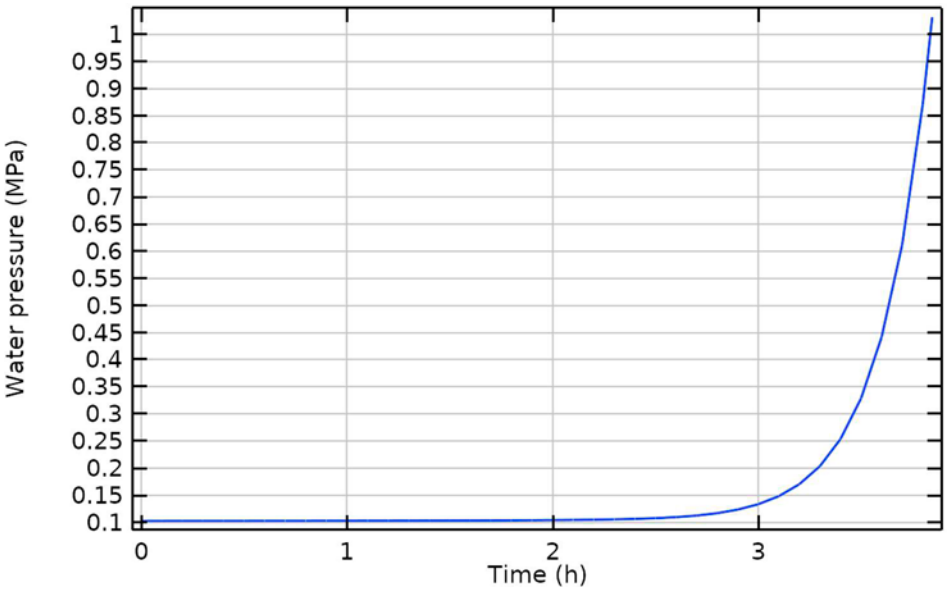

Figure 7-17. *Inlet pressure evolution in the model.*

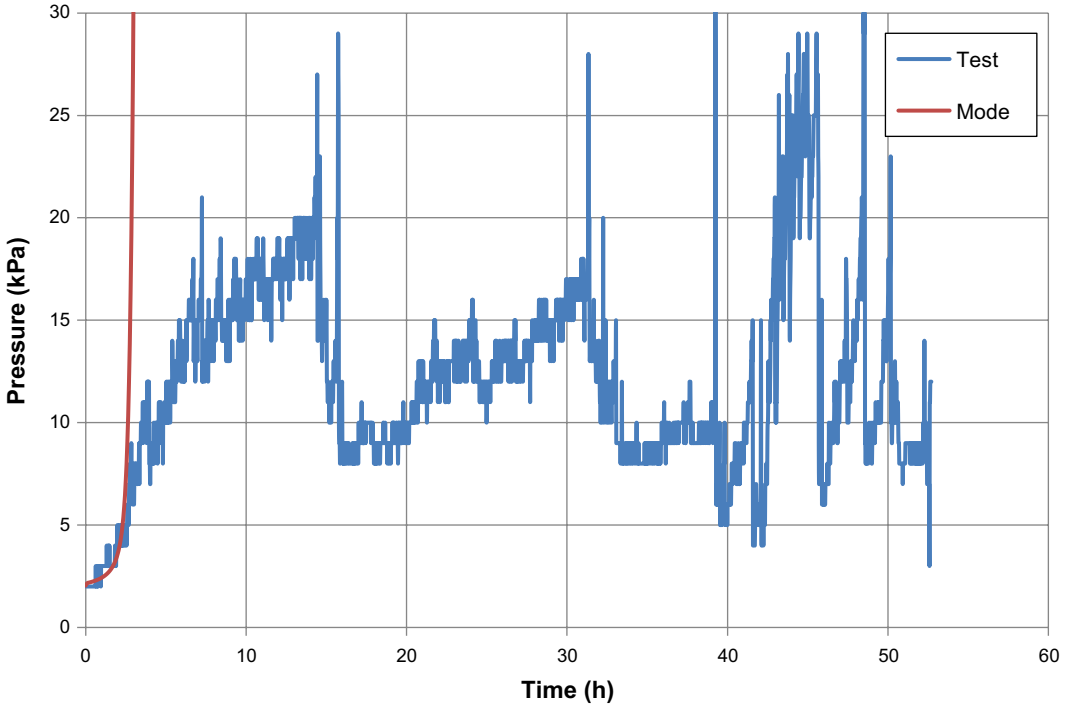

Figure 7-18. *Inlet pressure evolution (blue) in comparison with the model (red).*

7.4.4 Results 0.1 l/min

At the higher inflow the water can flow much further before the pellets starts to swell. Therefore the water will flow down to the bottom and continue to fill from the bottom up. Due to that the Darcy has a tendency to spread the water the down flowing seems to be wider in the model, se Figure 7-19.

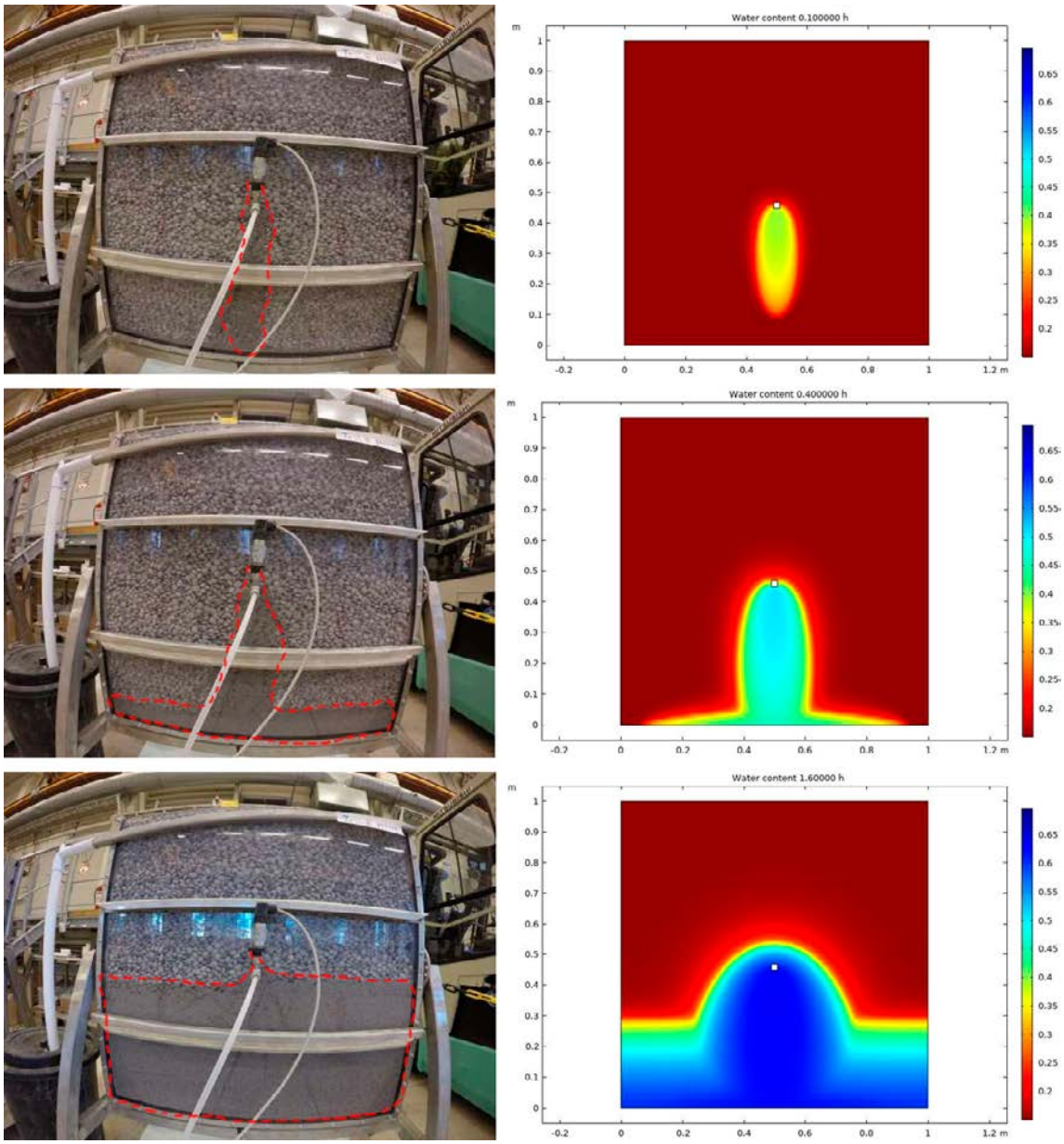

Figure 7-19. *Wetting comparison between model and test at the inflow of 0.1 l/min*

Conclusions

A model for describing water transport in pellet fillings has been developed. The model seems to be able to predict most transport processes of water that occur in the pellet fillings. The model includes physics to describe suction gradient driven transport vapour transport both due to diffusion and due to convection in the pellets fillings and also the ability to model transport of free water in between the pellets. Although the model gives rather good results for the test cases used in this report there are a need to further test the model and find out how well it performs in different situations. Since the model does not include the formation of pipes in the pellet filling there is a limitation to use the model at lower inflows that takes place during longer periods. Some representation of the piping should be added to the model to get a more complete model.

References

SKB's (Svensk Kärnbränslehantering AB) publications can be found at www.skb.com/publications.

Denny M W, 1993. Air and water: the biology and physics of life's media. Princeton: Princeton University Press

Dueck A, Nilsson U, 2010. Thermo-hydro-mechanical properties of MX-80. Results from advanced laboratory tests. SKB TR-10-55, Svensk Kärnbränslehantering AB.

Eriksson P, 2017. Compaction properties of bentonite clay. SKB TR-16-16, Svensk Kärnbränslehantering AB.

Johnsson A, Sandén T, 2013. System design of backfill. Pellet optimization. SKB R-13-47, Svensk Kärnbränslehantering AB.

Lundgren C, Johannesson L-E, 2020. Optimering av buffertpellets för KBS3. Laboratorieförsök på fyra olika pellets. SKB R-19-25, Svensk Kärnbränslehantering AB.

Luterkort D, Johannesson L-E, Eriksson P, 2017. Buffer design and installation method Installation report. SKB TR-17-06, Svensk Kärnbränslehantering AB.

Sandén T, Olsson S, Andersson L, Dueck A, Jensen V, Hansen E, Johnsson A, 2014. Investigation of backfill candidate materials. SKB R-13-08, Svensk Kärnbränslehantering AB.

Svensson D, Lundgren C, Johannesson L-E, Norrfors K, 2017. Developing strategies for acquisition and control of bentonite for a high level radioactive waste repository. SKB TR-16-14, Svensk Kärnbränslehantering AB.

Svensson D, Eriksson P, Johannesson L-E, Lundgren C, Bladström T, 2019. Development and testing of methods suitable for quality control of bentonite as KBS-3 buffer and backfill. SKB TR-19-25, Svensk Kärnbränslehantering AB.

Arkitektkopia AB, Bromma, 2020

SKB is responsible for managing spent nuclear fuel and radioactive waste produced by the Swedish nuclear power plants such that man and the environment are protected in the near and distant future.

skb.se